Lithos 246–247 (2016) 165–181

Contents lists available at ScienceDirect

Lithos

journal homepage: www.elsevier.com/locate/lithos

Late Cretaceous UHP metamorphism recorded in kyanite–garnet schists from the Central Rhodope Mountains, Bulgaria

David Collings [a], Ivan Savov [a,*], Kathryn Maneiro [b], Ethan Baxter [b,c], Jason Harvey [a], Iliya Dimitrov [d]

[a] School of Earth and Environment, University of Leeds, Leeds, UK
[b] Department of Earth and Environment, Boston University, Boston, USA
[c] Department of Earth and Environmental Sciences, Boston College, Boston, USA
[d] National Museum of Natural History, Sofia, Bulgaria

ARTICLE INFO

Article history:
Received 16 October 2015
Accepted 6 January 2016
Available online 20 January 2016

Keywords:
Ultra high pressure
Kyanite–garnet schist
Rhodope
Bulgaria
Diamond

ABSTRACT

In this study, we report the first discovery of microdiamond inclusions in kyanite–garnet schists from the Central Rhodope Mountains in Bulgaria. These inclusions occur in garnets from metapelites that are part of a meta-igneous and meta-sedimentary mélange hosted by Variscan (Hercynian) orthogneiss. Ultra-high-pressure (UHP) conditions are further supported by the presence of exsolved needles of quartz and rutile in the garnet and by geothermobarometry estimates that suggest peak metamorphic temperatures of 750–800 °C and pressures in excess of 4 GPa. The discovery of UHP conditions in the Central Rhodopes of Bulgaria compliments the well-documented evidence for such conditions in the southernmost (Greek) part of the Rhodope Massif. Dating of garnets from these UHP metapelites (Chepelare Shear Zone) using Sm–Nd geochronology indicates a Late Cretaceous age (70.5–92.7 Ma) for the UHP metamorphic event. This is significantly younger than previously reported ages and suggests that the UHP conditions are associated with the Late Mesozoic subduction of the Vardar Ocean northward beneath the Moesian platform (Europe). The present-day structure of the RM is the result of a series of subduction–exhumation events that span the Cenozoic, alongside subsequent post-orogenic extension and metamorphic core complex formation.

1. Introduction

It is now widely accepted that in convergent margin settings, rocks can be subducted to depths exceeding 150 km and then returned to the surface. Recognition of this deep subduction–exhumation cycle followed the discovery of coesite in rocks from the Dora Massif in the Western Alps (Chopin, 1984) and discovery of microdiamonds in the Kokchetav Massif of Kazakhstan (Sobolev and Shatsky, 1990). Although rare, in recent years, further discoveries of ultra-high-pressure (UHP) indicators (diamond, coesite) have been made worldwide (Dobrzhinetskaya, 2012). Ultra-high-pressure rocks have proven to be of great importance as natural archives of the mineralogy and conditions (temperature, pressure, % volatiles, among others) of the deeply subducted lithosphere that complement prior insights from high-pressure experimental petrology.

This study investigates metapelitic kyanite–garnet schists from the Rhodope Massif (RM) in Bulgaria. The RM is a crustal-scale duplex complex that straddles the Bulgarian–Greek border and represents the manifestation of the Alpine Orogeny in southeastern Europe (Burg, 2012; Ricou et al., 1998). The RM is composed of a series of mountain ranges (Western, Central, and Eastern Rhodope Mountains see Fig. 1) that record a multi-stage, post-Proterozoic tectonic evolution (Burg, 2012; Haydoutov et al., 2004; Ivanov et al., 1985; Ricou et al., 1998), although the majority of the subduction and/or collisional events record Jurassic to Eocene closure of the Paleotethys and/or the Tethys Ocean (Bonev and Stampfli, 2011; Ricou et al., 1998). Three discoveries of microdiamonds have now been reported from the southern rim of the RM, establishing the massif as a globally important UHP locality (Mposkos and Kostopoulos, 2001; Perraki et al., 2006; Schmidt et al., 2010). All three examples of microdiamonds are found as inclusions in garnets from metapelitic units in Greece, leaving the full extent of UHP conditions in the remaining parts of the RM (>3/4 of which are in Bulgaria) as unknown.

Here, for the first time, we report the composition and metamorphic evolution of UHP units from the Bulgarian part of the RM. We report the timing of the UHP event on the basis of new high quality Sm–Nd garnet geochronology. The relationship of the metamorphic rocks recording the UHP conditions with other known high-pressure (including UHP) localities in the region, as well as the host gneisses and melange rocks, are also considered, and the implications of this discovery on the tectonic evolution of the RM and the adjacent terrains are discussed.

* Corresponding author.
E-mail address: i.savov@see.leeds.ac.uk (I. Savov).

http://dx.doi.org/10.1016/j.lithos.2016.01.002

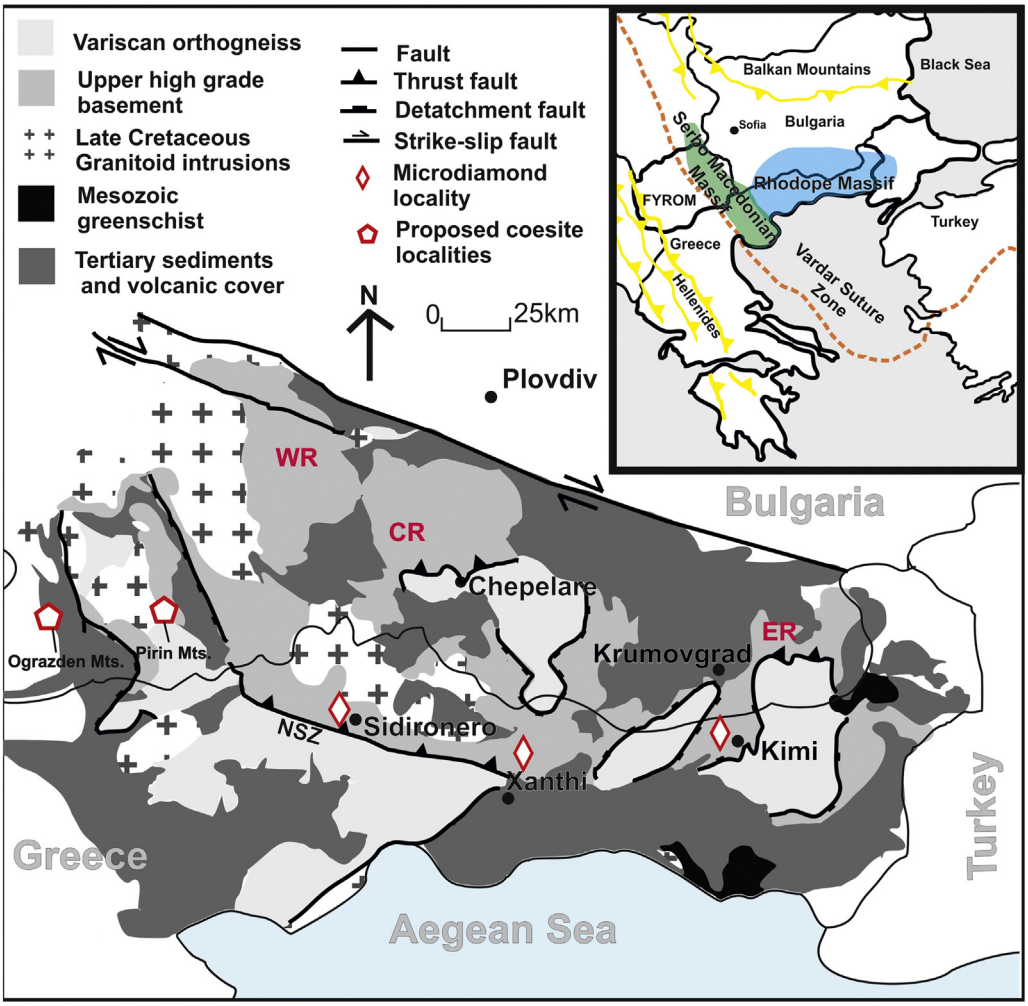

Fig. 1. Summary map of the geology of the Rhodope Massif (after Bonev et al., 2006 and Bonev and Stampfli, 2008). ER: Eastern Rhodope Mountains; CR: Central Rhodope Mountains; WR: Western Rhodope Mountains; NSZ: Nestos Shear Zone; CSZ: Chepelare Shear Zone.

2. Geological setting

2.1. Regional geology

The RM forms the innermost part of the Hellenides, extending over large areas of Southern Bulgaria and NE Greece (Fig. 1). It is bounded to the north by the Sredna Gora Zone, a Late Cretaceous volcanic arc chain of granite–monzodiorite intrusions (Von Quadt et al., 2005), which is separated from the RM by the Maritza dextral strike-slip fault (Naydenov et al., 2009). To the west, it is bounded by the Serbo-Macedonian Massif (SMM)/Vardar Suture Zone (Ricou et al., 1998), and the eastern boundary is covered by the large, late Paleogene–Neogene Thrace-Maritza sedimentary basin and the Circum Rhodope belt.

The RM was originally considered a Precambrian crustal entity sandwiched between two branches of the Alpine–Himalayan orogenic belt with the Balkan belt to the north and the Dinarides–Hellenides belt to the south (Hsu et al., 1977). Subsequent work instead indicates a more complex evolution, with Precambrian, Variscan, and Alpine metamorphic and igneous activity (Bonev and Stampfli, 2008, 2010; Burchfiel, 1980; Carrigan et al., 2003; Haydoutov et al., 2004; Ivanov et al., 1985) followed by extensive Alpine deformation and complex extensional tectonics (Baziotis et al., 2008; Bonev et al., 2006; Burg, 2012; Burg et al., 1996; Ivanov et al., 1985; Ricou et al., 1998). The current interpretation indicates that the RM is a south directed nappe complex formed as a result of a north dipping Cretaceous subduction zone associated with the closure of the Vardar Ocean (Ricou et al., 1998). By the Late Eocene-Miocene, the RM experienced post-orogenic extension, which led to the emplacement of a series of large-scale metamorphic domes (core complexes) that dominate the regional geology (Bonev et al., 2006, 2010; Burg et al., 1996; Ivanov et al., 1985).

2.2. Stratigraphy and lithotectonic structure of the Rhodope Massif

A number of different classifications have been used for lithological units across the RM, which often precludes direct comparisons between regions/mountain ranges. In recent years, two simplifications of the geology have been proposed to group units that share a common formation history and/or lithology. The first scheme, as proposed by Bonev et al. (2006), divides the metamorphic basement into two units: an upper high-grade basement and a lower high-grade basement, whereas the second scheme divides the metamorphic basement into four distinct units: the lowermost, middle, upper, and uppermost allochthons (Jahn-Awe et al., 2010).

The lower high-grade basement unit and lower allochthon are the same in both classification schemes and are predominantly orthogneiss with associated metasediments, metamafic, and ultramafic rocks (Bonev et al., 2006; Jahn-Awe et al., 2010). The largest exposures of the lower allochthon are in the Pangeon–Pirin complex, outcropping south of the Netsos Shear Zone in Northern Greece/Southern Bulgaria, as well as in the cores of the three large extensional gneiss domes (Arda, Byala-Reka, and Kesebir-Kardamos; see Fig. 1) that shape the present-day topography and tectonic structure of the RM.

The next stratigraphic level in the RM is an extensive heterogeneous unit of meta-igneous and meta-sedimentary rocks (mélange) of currently unresolved age and origin. This suite is the focus of this study. Ricou et al. (1998) and Bonev et al. (2006) both grouped all lithological units at this level together into the Rhodope Terrane and upper high-grade basement unit, respectively, whereas Jahn-Awe et al. (2010) subdivided it further into a middle and upper allochthon on the basis of contrasting protolith ages and tectono-metamorphic histories.

The middle allochthon is composed of intermingled amphibolites, marbles, eclogites, metapelites, variously serpentinized ultramafics, and ortho- and para-gneisses that have experienced upper amphibolite/eclogite facies metamorphism. Late Jurassic–Early Cretaceous protolith ages have been reported for orthogneiss in the middle allochthon from both above the Nestos Shear Zone (Turpaud and Reischmann, 2010) and the eastern extent of the Arda dome (Ovtcharova et al., 2004). The upper allochthon is petrologically similar but is proposed to represent a higher stratigraphic level in the RM, containing all of the previously reported examples of UHP metamorphism in the RM (Jahn-Awe et al., 2010). The timing of metamorphism in this allochthon is poorly constrained. The exact criteria for inclusion of a rock assemblage in either the middle or upper allochthon is not clear in the literature, but the mélange zone found along the Nestos and Chepelare Shear Zones and the Kimi complex of the Eastern Rhodope Mountains have all been assigned to the upper allochthon (Jahn-Awe et al., 2010; Jahn-Awe et al., 2012; Nagel et al., 2011). For the purpose of this study, both units, the middle and the upper allochthons, will be referred to as the Variegated Formation (VF), a term used locally in the Bulgarian Rhodope Mountains (Haydoutov et al., 2004).

Overlying the VF are a series of Mesozoic greenschist–blueschist grade metasediments and metavolcanics, thought to be a continuation of the Circum Rhodope belt from the Athos–Volvi zone, Greece (Boyanov and Russeva, 1989; Papanikolaou, 1997). This upper high-grade basement unit, or uppermost allochthon, is composed of greenschists and phyllites overlain by arc tholeiitic and boninitic lavas, which are in turn overlain by meta-pyroclastic rocks, turbidites, and carbonates (Bonev et al., 2010). The entire sequence is overlain by a series of syn- and post-tectonic sequences. These supracrustal units consist of clastic, carbonaceous, and volcanic materials with ages ranging from Paleocene to Miocene (Boyanov and Goranov, 2001). The widespread post-metamorphic magmatic activity has been related to post-orogenic extensional collapse (Harkovska et al., 1989; Jones et al., 1992), likely a result of slab rollback due to a change in composition of the subducting crust (Georgiev et al., 2012; Jolivet and Brun, 2010).

This study focuses on the metamorphic history of the VF in the vicinity of the town of Chepelare, on the edge of the large Arda gneiss dome (25 × 25 km) in the Central Rhodope Mountains Here, the Variscan orthogneisses from the lower high-grade units can be divided into two distinct sub-units—"Arda 1" and "Arda 2", with the boundary between these units interpreted as a high strain shear zone or syn-metamorphic thrust fault (Ivanov et al., 1985; Ricou et al., 1998; Burg, 2012; this study, see Fig. 2). There is little field evidence to differentiate the two sub-units, with the exception of a series of meter-scale elongate eclogite boudins that occur throughout the upper parts of the Arda 2 subunit. Beneath the syn-metamorphic thrust fault, the VF is represented by a heterogeneous sequence of meta-igneous and meta-sedimentary rocks hosted by the Variscan Arda 1 gneiss (Cherneva and Georgieva, 2005). The VF has an irregular outcrop pattern in a zone of intense deformation wrapping around the Arda 1 unit (Fig. 2). Marble is the most abundant lithology within the VF, followed by amphibolites and kyanite–garnet schists, the subject of this study.

The RM has been tectonically active since at least the Carboniferous/Permian times, when the area experienced widespread igneous activity (Burg, 2012; Cherneva and Georgieva, 2005; Liati, 2005; Liati et al., 2011; Turpaud and Reischmann, 2010). Granites emplaced during this period formed the orthogneiss protolith of the lower high-grade RM basement. Metagabbro and eclogite included in the Variscan gneiss as lenses and boudins also yield Precambrian and Early Paleozoic protolith formation ages (generally >500 Ma; Savov et al., 2007) and evidence for a metamorphic overprint ca. 350 Ma (Carrigan et al., 2003). The size and extent of this Variscan metamorphic event and the relationship with the rest of the RM remains enigmatic (Burg, 2012), although segments of a Precambrian-Paleozoic (Variscan) suture have already been identified in the Eastern RM near the Bulgarian–Greek–Turkey border (Haydoutov et al., 2004).

2.3. UHP metamorphism in the Rhodope Massif

In the last decade, the RM has been the focus of extensive research due to the discovery of microdiamond inclusions in garnets from kyanite–garnet gneiss/schist of the Kimi Complex, part of the upper high-grade basement in the Greek part of the RM (Mposkos and Kostopoulos, 2001). Two additional diamond localities have since been identified along the Nestos Shear Zone in the South of the RM (Fig. 1) and in the Sidironero Complex (Perraki et al., 2006; Schmidt et al., 2010). These discoveries have established the region as a globally important UHP province. Microdiamond inclusions are restricted to almandine-rich garnets from kyanite–garnet gneiss/schist units that are part of the VF/Upper allochthon (mélange) that is common throughout the upper high-grade basement unit of the RM (Haydoutov et al., 2004). Kyanite–garnet gneiss/schist is the only lithology found to preserve evidence of UHP conditions. Pressure and temperature estimates for the Greek UHP localities range between 3.1 and 3.9 GPa and 600–900 °C for the Greek Central Rhodope Mountains and >4 GPa and at least 1100 °C for the Greek Eastern Rhodope Mountains (Liati et al., 2011). Thermobarometric studies of eclogites from the westernmost segments of the RM in Bulgaria (i.e. Pirin Mountains; Janak et al., 2011) and the coesite from the neighboring Ograzden Mountains of the Serbo-Macedonian Massif (Savov et al., 2007; Zidarov et al., 1995) suggest that other parts of the RM and its surroundings may have experienced UHP conditions.

2.4. Timing of UHP metamorphism

In recent years, a large number of geochronological studies have been conducted across the RM, utilizing a variety of dating techniques. A summary of all published metamorphic ages from the RM is presented in Table 1. Given the pulsed nature of the metamorphic record and the comparatively few geochronological studies that have been performed on UHP metapelitic units, a number of uncertainties remain surrounding the timing of the UHP metamorphic events(s). A recent review paper by Liati et al. (2011) suggested 4 HP events at ca. 150 Ma, ca. 73 Ma, ca. 51 Ma, and ca. 42 Ma, all of which could have attained UHP metamorphic conditions. In the Liati et al. (2011) study, the Jurassic (ca. 150 Ma) was favored as the most likely time for UHP metamorphism due to the lack of extensive recrystallization of the ca. 150 Ma zircon domain, which would be expected with subsequent UHP metamorphism. However, Liati et al. (2011) noted that a Jurassic UHP event fails to explain the preservation of microdiamond inclusions and exsolution textures within garnets in the same samples. Therefore, all four previously mentioned pulses (ca. 150 Ma, ca. 73 Ma, ca. 51 Ma and ca. 42 Ma) remain strong candidates for the timing of the UHP metamorphism.

Garnet dating has not been widely used to constrain the timing of UHP metamorphism in the RM. Only one study dated garnets from a UHP metapelite (Reischmann and Kostopoulos, 2002), yielding an age of 140 ± 4 Ma. Dating of associated metabasic samples produced Neoproterozoic and Carboniferous ages, interpreted as remnants of the Pan African and/or the Variscan orogeny (Carrigan et al., 2005; Savov et al., 2007) unrelated to the UHP metamorphic event.

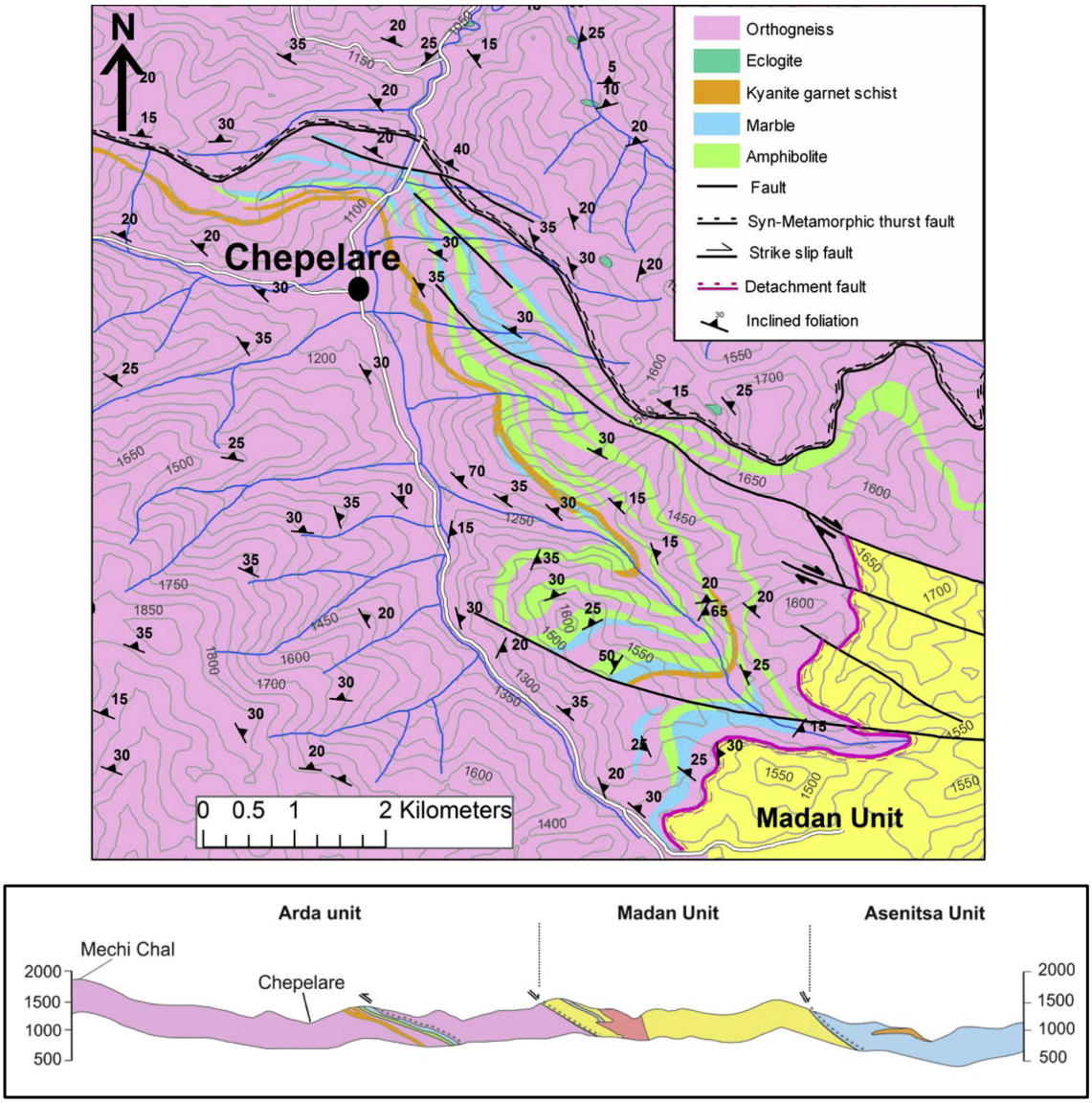

Fig. 2. Simplified geological map for the vicinity of the town of Chepelare in the Central Rhodope Mountains, Bulgaria, and schematic cross-section running N–S through the Arda Dome (redrawn from Sarov, 2004).

2.5. Petrography of kyanite–garnet schists from the Variegated Formation

In the vicinity of the town of Chepelare, kyanite–garnet schists outcrop as decimeter to meter sized packages found in close association with marbles, amphibolites, and gneisses, although contacts are often masked by vegetation or erosion. Where observed, the pervasive foliation of the kyanite–garnet schist follows that of the host Variscan gneisses. Alteration is widespread and many of the best specimens originate from abandoned exploration trenching or riverbeds. Five kyanite–garnet schist samples were collected for analysis from within the VF in the vicinity of Chepelare (for GPS locations see supplementary information).

Widespread textural and mineralogical variation is seen between individual samples—specimens can be grouped by garnet size, color, or relative abundance of key index minerals. A group of samples form a phaneritic end member with no visible matrix, containing only large, deep purple colored garnets, and elongated (up to 8 cm long) kyanite crystals (Fig. 3A, C), whereas another group are dominated by platy biotites that define a well-developed foliation alongside plagioclase, rutile, K-feldpsar, white mica, apatite, and pyrite (Fig. 3D). Other samples appear more migmatitic, with a weak foliation and a larger proportion of felsic minerals (Fig. 3B, E). Sillimanite is rare, but observed in some samples.

Among all samples, garnet color ranges from light pink to deep purple and size varies from <1 mm to >2 cm in diameter. Inclusions of quartz, rutile, and biotite are abundant in all samples, although inclusions are often restricted to distinct zones within a crystal. Rarer inclusions of muscovite, apatite, zircon, monazite, chlorite, and carbon can be found in the majority of the garnet samples (Fig. 3F, G). Oriented needles of rutile and biotite alongside rods of quartz are also not uncommon (Fig. 3 G).

Kyanite ranges from small, hard to distinguish needles <1cm in length to large porphyroblastic crystals up to 7 cm long. Crystals are commonly deformed, exhibiting both kink-banding and undulose extinction alongside retrogression to sericite along crystal rims. Inclusions of zircon, rutile, biotite, and muscovite are common within kyanite (Fig. 3H).

Two samples (3-1-10 and 38-1-11) have a matrix dominated by platy biotite crystals that define a well-developed foliation. Biotite is seen to wrap around garnet and kyanite porphyroblasts and is commonly retrogressed to chlorite and kaolinite, and in places fibrous sillimanite. Samples 27-1-10 and 2-1-11 have a matrix dominated by

Table 1
Summary of all available published metamorphic ages for the Rhodope Massif. E-RM: Eastern Rhodope Mountains; C-RM: Central Rhodope Mountains; GC: Greece; BG: Bulgaria; OMP: omphacite; Grt: Garnet.

Age (Ma)	Error (±Ma)	Rock type	Location	Dating technique	Reference
567		Eclogite	C-RM BG	Lu–Hf Grt–Omp	Savov et al. (2007)
~300		Metagabbro	E-RM BG	U–Pb zircon	Carrigan et al. (2003)
~300		Eclogite	C-RM BG	Lu–Hf Grt–Omp	Savov et al. (2007)
~186		Metapelite	C-RM GC	U–Pb Monazite	Reischmann and Kostopoulos (2002)
171	1	Metapelite	E-RM GC	U–Pb zircon	Bauer et al. (2007)
~160		Eclogite	E-RM GC	U–Pb zircon	Bauer et al. (2007)
160	1	Metapelite	E-RM GC	U–Pb zircon	Bauer et al. (2007)
153	13	Amphibolite	C-RM GC	Sm–Nd Grt	Kostopolous, in Burg (2011)
~150		Garnet gneiss	E-RM GC	U–Pb zircon	Liati et al. (2011)
~150		Metapelite	C-RM BG	U–Pb Monazite	Didier et al. (2014)
148.8	2.2	Paragneiss	C-RM GC	U–Pb zircon	Liati (2005)
147.2	4.7	Paragneiss	C-RM GC	U–Pb zircon	Liati (2005)
143.4	3.3	Eclogite	C-RM GC	U–Pb zircon	Liati (2005)
~140		Metapelite	C-RM BG	U–Pb monazite	Bosse et al. (2010)
140	4	Metapelite	C-RM GC	Sm–Nd Grt	Reischmann and Kostopoulos (2002)
~130		Metapelite	C-RM GC	U–Pb zircon	Krenn et al. (2010)
126	0.7	Eclogite	C-RM BG	Lu–Hf Grt	Kirchenbaur et al. (2012)
119	3.5	Garnet–pyroxenite	E-RM GC	Sm–Nd Grt	Wawrzenitz and Mposkos (1997)
117	1.9	Garnet amphibolite	E-RM GC	U–Pb zircon	Liati et al. (2002)
~115		Eclogite	E-RM GC	U–Pb zircon	Bauer et al. (2007)
82.8	1.3	Paragneiss	C-RM GC	U–Pb zircon	Liati (2005)
79	3	Eclogite	E-RM GC	U–Pb zircon	Bauer et al. (2007)
~77		Pegmatites	C-RM GC	U–Pb zircon	Bosse et al. (2009)
73.9	0.8	Garnet gneiss	E-RM GC	U–Pb zircon	Liati et al. (2011)
73.5	3.4	Grt amphibolite	E-RM GC	U–Pb zircon	Liati et al. (2002)
72.9	1.1	Pyroxenite	E-RM GC	U–Pb zircon	Liati et al. (2002)
71.4	1.1	Orthogneiss	E-RM GC	U–Pb zircon	Liati et al. (2011)
55.9	7.2	Orthogneiss	C-RM BG	U–Pb zircon	von Quadt et al. (2006)
51	1	Garnet amphibolite	C-RM GC	U–Pb zircon	Liati and Fanning (2005)
~50		Metapelite	C-RM BG	U–Pb monazite	Didier et al. (2014)
49.1	6	Metagabbro	E-RM BG	U–Pb zircon	Bonev et al. (2010)
~43		Eclogite	C-RM BG	Lu–Hf Grt	Kirchenbaur et al. (2012)
42.4	1.4	Pyroxenite	C-RM GC	U–Pb zircon	Liati et al. (2011)
42.2	0.9	Amp eclogite	C-RM GC	U–Pb zircon	Liati et al. (2002)
42.1	1.2	Pegmatites	C-RM BG	U–Pb Monazite	Bosse et al. (2009)
~40		Leucosome	C-RM GC	U–Pb zircon	Liati et al. (2002)
~40		Metapelite	C-RM BG	U–Pb Monazite	Bosse et al. (2010)
39.7	1.2	Lecuosome	C-RM GC	U–Pb zircon	Liati (2005)
38.1	0.8	Garnet amphibolite	C-RM GC	U–Pb zircon	Liati (2005)

quartz, occurring in two forms. The most widespread samples are interlocking quartz grains (100–500 μm in diameter) that exhibit undulose extinction, grain boundary migration, and bulging, with the remainder being recrystallized quartz with a granoblastic mortar texture, often found in close association with biotte and chlorite. Finally, sample 47-1-11 has no clear matrix, with only small pockets of fine-grained aggregates of quarts and decussate biotite forming between the larger porphyroblasts.

The original high-pressure assemblage was likely garnet + kyanite + phengite + quartz + rutile, which has been later overprinted by the post-peak assemblage (biotite + plagioclase + K-feldspar + chlorite + white mica) (Collings, 2014).

3. Analytical techniques

3.1. Petrology and mineral chemistry

Mineral-scale textures and particularly small mineral inclusions (<50 μm) were investigated at the University of Leeds on a FEI Quanta 650 FEG-ESEM. The chemical compositions of the major rock-forming minerals were determined via electron microprobe analysis at the University of Leeds, using a JEOL 8230 electron microprobe analyzer (EMPA). A range of analytical conditions were used, optimized for individual mineral targets. An accelerating voltage of 15 kV was used, with spot sizes ranging between 2 μm and 5 μm. For Zr in rutile thermometry, the EPMA was optimized for analysis of trace amounts of Zr, with Zr analyses performed simultaneously on three spectrometers. A 50-nA beam with an accelerating voltage of 15 kV, and a count time of 60 seconds was used for each analysis.

3.2. Laser Raman spectroscopy

In order to identify possible diamond grains, a Renishaw 2000 Raman microscope with a HeNe laser operating at 633nm was used at the University of Leeds Laser Raman Spectroscopy Facility. The laser was focused using the ×50 objective lens to a 2- to 3-μm spot and was operated at 100% power.

3.3. Garnet geochronology

3.3.1. Sample preparation

Sm–Nd garnet geochronology was performed on five samples at the Boston University TIMS facility. Samples were crushed using a steel hammer and anvil, followed by handpicking of approximately 0.1 g of garnet. After further crushing in a tungsten carbide pestle and mortar to a grain size between 106 μm and 63 μm, separation by Frantz magnetic separator, and a final stage of handpicking, samples underwent a three-stage partial dissolution technique using hydrofluoric, perchloric, and nitric acids to remove any remaining matrix minerals besides garnet and mineral inclusions within the garnet. The partial dissolution procedure followed Baxter et al. (2002) and subsequent modifications by Pollington and Baxter (2011) and Dragovic et al. (2012). Once clean, garnet samples underwent full dissolution following the steps outlined in Harvey and Baxter (2009). Whole rock samples were first digested using Parr 4749 general-purpose acid digestion

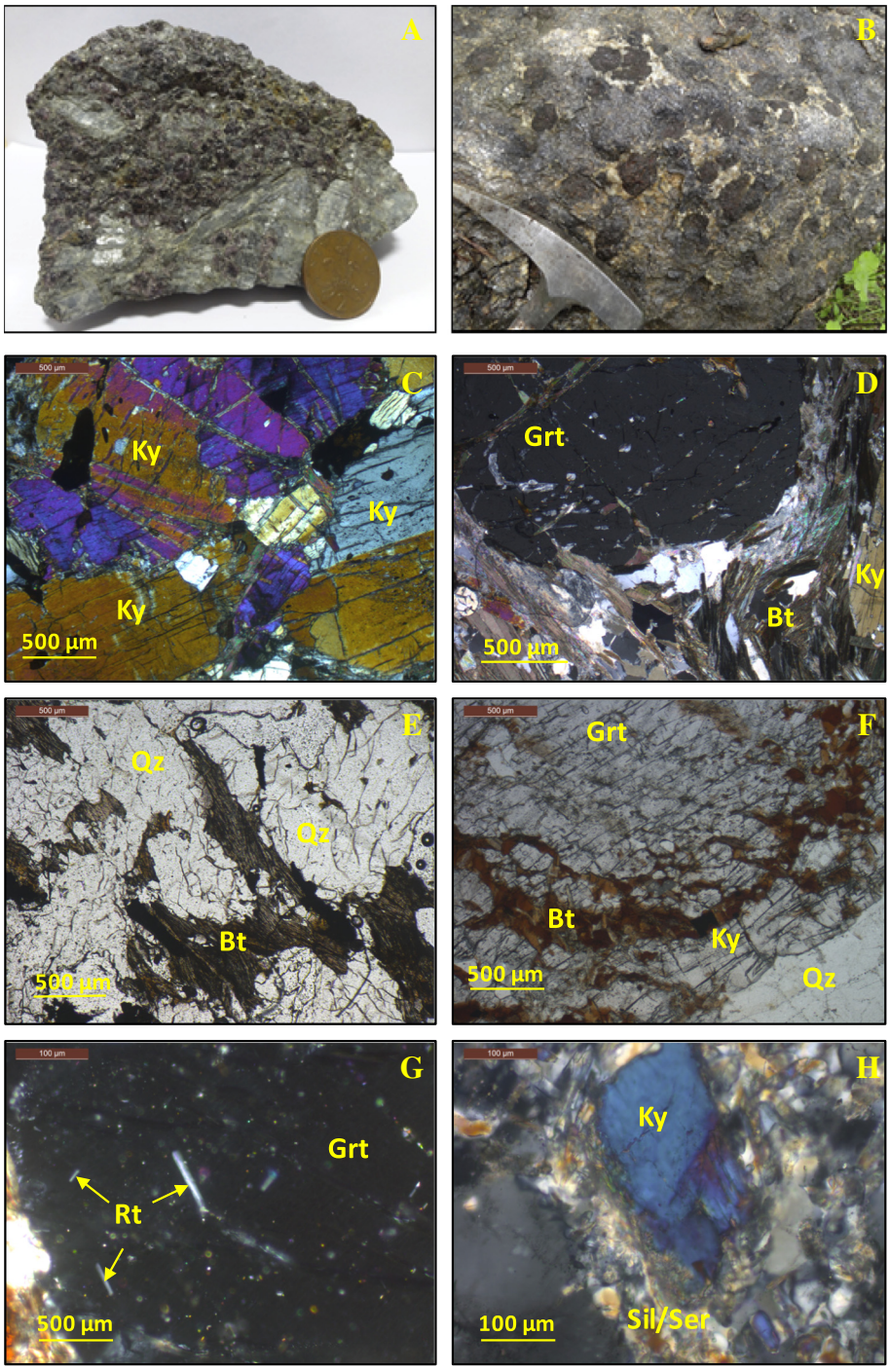

Fig. 3. (A) Photograph of a phaneritic kyanite–garnet schist sample from the vicinity of Chepelare with no visible matrix. (B) Photograph of magmatic sample with a quartz rich matric and large garnet porphyroblasts. (C) Interlocking kyanite crystals in phaneritic end member kyanite–garnet schist (sample 47-1-11). (D) Intact garnet with exsolved needles of rutile, with platy biotite matrix wrapping around garnet crystal (sample 3-1-10). (E) Quartz and biotite matrix in migmatitic sample (35-1-11). (F) Retrogressed garnet and kyanite, with quartz lens in matrix (sample 27-1-10). (G) Oriented rutile needles exsolved within a garnet crystal (sample 27-1-10). (H) Matrix kyanite crystal breaking down to form sillimanite/sericite (sample 27-1-10).

bombs then dissolved using the same full dissolution procedure as the garnet with extended time in acid to ensure full dissolution of each sample. All samples were spiked with a mixed ^{147}Sm–^{150}Nd spike and underwent chromatographic separation on a series of three columns: a column containing cation exchange resin (AG50w-X4) to remove Fe, a Teflon microcolumn containing Eichrom TRU-spec resin to isolate the rare earth elements, and a Teflon column containing cation exchange resin and using 2-methyllactic acid (MLA) column to separate Sm and Nd.

In addition to aggregate garnet analysis, four large garnet porphyroblasts were extracted from kyanite–garnet schist samples from the Central Rhodope Mountains. These were cut through the geometric centre of the crystal and polished to form a 2-mm thick polished wafer. Samples were mapped for Ca, Mg, Fe, and Mn via EPMA at the University of Leeds (Fig. 4). A grid spacing of 250 µm was used for all samples. The probe was operated at an accelerating voltage of 15KV, a probe current of 150 nA, and a counting time of 5s for each of the 4 major cations.

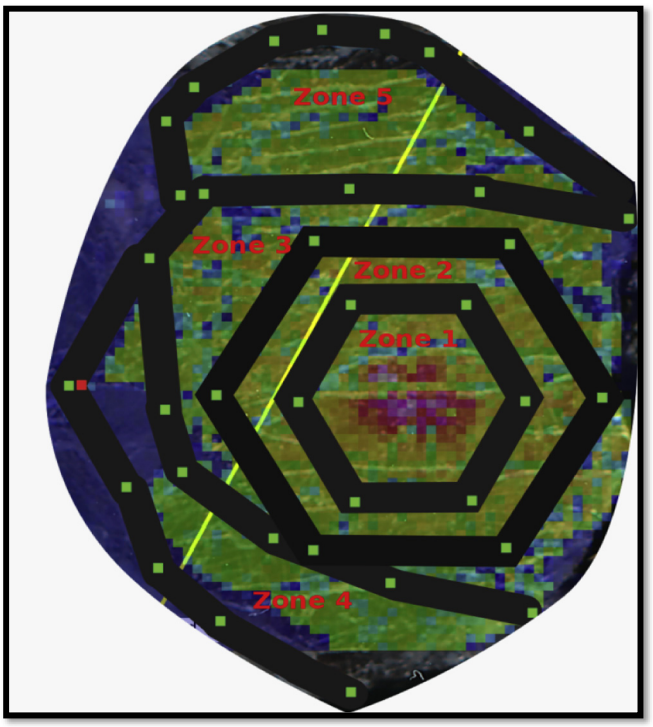

Fig. 4. Elemental Mn map of large garnet crystal from sample 27-1-10. Trenches for micromilling alongside points used for micromilling are also shown. Length of yellow line is 2.5 cm.

One of these large garnets was selected for microsampling at Boston University, following the procedures outlined in Pollington and Baxter (2011) and Dragovic et al. (2012). Using the Mn elemental map (Fig. 4), five zones were defined and drilled using a NewWave MicroMill. The garnet wafer was attached to a graphite block using Crystal Bond, allowing easy removal with acetone with minimal risk of Nd contamination due to the very low concentrations of Nd in Crystal Bond. The block was surrounded by a water-tight Teflon ring, and the sample was submerged in milli-Q water during drilling. Multiple traverses were performed along pre-defined paths to drill out the trenches, with each pass drilling 50 μm deep. Five trenches were drilled to isolate the five garnet zones (Fig. 4). Once extracted, each zone underwent the same hand-crushing, magnetic separation, partial dissolution, and chemical separation techniques previously described for the aggregate garnet samples.

3.3.2. Sample analysis

All samples were analyzed using a Thermo Finnigan TRITON TIMS instrument at the Boston University TIMS facility. Nd separates were loaded onto single Re filaments using 1 μl of 2 M HNO_3 with 2 μl of H_3PO_4 and Ta_2O_5 activator slurry, as described in Harvey and Baxter (2009). The mass spectrometer was run in static mode with amplifier rotation, and Nd was measured as NdO^+. Repeat 4-ng analyses of our in-house Nd standard solution (Ames metal) during the course of analysis yielded a mean of $^{143}Nd/^{144}Nd = 0.512132 \pm 0.000016$ (31 ppm, 2 RSD, $n = 35$).

The reproducibility in $^{147}Sm/^{144}Nd$ is 0.023% (2 RSD) based on repeat analyses of a mixed gravimetric normal solution with our calibrated in-house spike. Whole procedural blanks ranged between 13 and 26 pg for Nd, and around 3 pg for Sm. The Nd blank value for the bombed whole rock sample was 171 pg, which although high is insignificant in comparison to the large amount of Nd in the whole rock solution. Three column blanks ranged between 12 and 20 pg for Nd and between 1.5 and 1.6 pg for Sm.

4. Results

4.1. Mineral chemistry

The major element chemistry of garnets from four garnet–kyanite (metapelitic) samples are presented in Table 2. All garnets are almandine rich ($Alm_{68–80}$) and display variable grossular ($Grs_{0.7–7.4}$), pyrope ($Prp_{6.8–22.9}$), and spessartine ($Sps_{0.8–6.6}$) contents. The compositional range within individual samples is small compared to that observed between samples. Individual garnet crystals preserve prograde Mn and Ca zonation (Fig. 4), although this is more pronounced in larger garnet crystals.

White mica analyses from two metapelites are presented in Table 3. All analyzed crystals are muscovite/phengite, with small amounts of paragonite and negligible margarite. Paragonite content varies, and although no trends are recognized between individual subgroups, two distinct populations of white mica can be identified on the basis of Na/(Na+K) ratios. Si content ranges from 3.03 to 3.63 a/fu, suggesting a variable phengite component.

Representative biotite analyses are shown in Table 4. Large variation (between 35 and 60) is seen in the Mg# of the biotite crystals. Biotite inclusions within garnet grains have particularly high Mg#, which likely reflects retrograde exchange reactions. Titanium content in biotite has previously been shown to increase as a function of metamorphic grade (Guidotti, 1984). Although little within-sample variation in titanium content is seen, biotite from samples 25-1-10 have both higher Ti and higher Mg# when compared with biotite from samples 3-1-10, indicating possible formation at higher metamorphic grades.

4.2. P-T history

4.2.1. Petrological constraints on P-T conditions

To date, there has been no reported direct evidence of UHP conditions (either coesite or microdiamond inclusions) in the Bulgarian part of the Rhodope Mountains Previous studies of Chepelare metapelites have suggested HP/UHP conditions (Georgieva et al., 2007; Kostopoulos et al., 2003) on the basis of observed exsolution of rutile and polyphase inclusions in garnet. These markers have also been recognized in this study (Fig. 3G), but additional microdiamond inclusions have been found in garnet, establishing the occurrence of UHP metamorphic conditions in the area.

A carbon inclusion was identified on the SEM (Fig. 5a), confirmed as carbon using EDS spectroscopy, and fluorescence was observed using the cathodoluminescence detector. Further, laser Raman spectroscopic investigation identified the inclusion as diamond, with the characteristic Raman spectra peak at 1333.2 cm^{-1} (Fig. 5d). Two methods were employed to ensure that the microdiamond was not an artifact from the polishing process. First, a study of the diamond polishing paste was conducted on the SEM. This revealed that the shape of the synthetic diamonds used in the polishing paste was euhedral, without the distinctive stepped cleavage observed in the diamond inclusion (Fig. 5c). Additionally, diamond pastes containing only 10 μm, 3 μm, and 1 μm diamonds were used in the polishing process i.e. the diamond inclusion of interest is not any of those sizes.

Second, an additional polished block of garnet separates from the same sample was prepared and polished with 0.3 μm alumina rather than diamond paste. A small carbon inclusion (Fig. 5b) (<1 μm) fluoresced under cathodoluminescence, revealing that it is not graphite. The texture of this inclusion resembles partially graphitized microdiamonds from the Kokchetav massif (Korsakov et al., 2010b) and the results of experimental studies on UHP diamond crystallisation performed by Dobrzhinetskaya (2012). The small size of the inclusion, however, rendered it unsuitable for confirmation by laser Raman spectroscopy. These observations suggest that kyanite–garnet schist from the Chepelare area experienced pressures of at least 4 GPa and reached depths in the crust in excess of 100 km.

Table 2
Summary of EPMA analyses of garnet from kyanite–garnet schist from the vicinity of Chepelare. Prp: pyrope content; Grs: grossular content; Alm: almandine content; Sps: spessartine content.

	3-1-10			2-1-10			25-1-10		47-1-11	
	Core	Middle	Rim	Core	Middle	Rim	Core	Rim	Core	Rim
SiO_2	37.09	37.13	37.02	37.68	37.6	37.5	37.55	37.54	37.59	37.36
TiO_2	0.01	0.01	0.02	0.01	0.01	0.01	0.03	0.06	0	0.01
Al_2O_3	21.02	21.1	21.05	21.05	20.95	21.03	21.32	21.26	21.26	21.2
Cr_2O_3	0.01	0.01	0.03	0.02	0	0.01	0.01	0.02	0.02	0.02
Fe_2O_3	0.22	0.06	0.01	0.51	0.6	0.36	0.74	0.68	0.41	0.52
FeO	35.88	35.93	36.01	35.32	35.47	35.91	32.53	32.96	31.18	32.14
MnO	1.69	1.72	2.36	0.46	0.49	0.56	0.74	0.83	0.69	0.89
MgO	2.73	2.66	2.18	4.35	4.04	3.63	5.28	4.77	5.78	5.04
CaO	1.73	1.77	1.7	1.25	1.46	1.51	2.15	2.39	2.58	2.67
Total	100.35	100.48	100.39	100.65	100.63	100.52	100.35	100.52	99.52	99.86
Si	2.99	2.99	2.99	3	3	3	2.97	2.97	2.98	2.97
Ti	0	0	0	0	0	0	0	0	0	0
Al	2	2	2	1.97	1.97	1.98	1.99	1.99	0.02	0.03
Cr	0	0	0	0	0	0	0	0	0	0
Fe^{3+}	0.01	0	0	0.03	0.04	0.02	0.04	0.04	0.02	0.03
Fe^{2+}	2.42	2.42	2.43	2.35	2.36	2.4	2.15	2.18	2.07	2.14
Mn	0.12	0.12	0.16	0.03	0.03	0.04	0.05	0.06	0.05	0.06
Mg	0.33	0.32	0.26	0.52	0.48	0.43	0.62	0.56	0.68	0.6
Ca	0.15	0.15	0.15	0.11	0.12	0.13	0.18	0.2	0.22	0.23
Total	8.01	8.01	8	8	8	8	8.01	8.01	8.01	8.02
Mg#	11.88	11.65	9.73	17.96	16.87	15.27	22.44	20.5	24.62	21.59
prp	10.97	10.69	8.77	17.22	16.04	14.47	20.96	18.94	22.93	20.1
grs	4.36	4.63	4.77	3.03	3.34	3.87	4.53	5.34	6.03	6
alm	80.19	80.27	80.91	78.19	78.7	79.93	71.24	72.35	68.16	70.22
Sps	3.86	3.93	5.4	1.03	1.11	1.27	1.66	1.88	2.0275	1.5628
n	18	14	34	5	4	11	18	33	11	7

4.2.2. Geothermometry

4.2.2.1. Zr-in-rutile thermometry. Peak temperatures experienced by the kyanite–garnet schists have been determined using the Zr-in-rutile thermometer of Tomkins et al. (2007). This thermometer is based upon the empirical relationship between Zr concentration in rutile and temperature of metamorphism, as identified by Zack et al. (2004) and takes into account the effect of pressure on this relationship. For the purposes of this study, a pressure of 40 kbar was assumed for all calculations. Rutile exsolved from garnet was ignored, as this rutile will not have equilibrated with quartz and zircon. Analysis was performed on two samples (3-1-10 and 25-1-10), and a summary of results can be found in the Supplementary material. Results were grouped in terms of textural setting. In sample 3-1-10, the Zr content of rutile ranges between 210 and 778 ppm, equating to temperatures between 723 and 849 °C, although average analyses of each textural setting have a narrower range of Zr content (353–437) equating to temperatures of 769–890 °C. In sample 25-1-10 the Zr content of rutile ranges between 250 and 1270 ppm, equating to temperatures of 738 and 905 °C. Again, average analyses from each textural setting have a narrower range of Zr content (352–564 ppm) equating to temperatures of 769–815 °C. No distinction can be made between

Table 3
Summary of EPMA data for white mica from Chepelare metapelites.

		3-1-10						25-1-10		
		Inclusion ($n = 89$)			Matrix ($n = 186$)			Matrix ($n = 17$)		
		Avg	Max	Min	Avg	Max	Min	Avg	Max	Min
Oxide wt %	SiO_2	47.11	50.88	44.66	48.53	56.47	44.27	48.7	51.85	47.07
	TiO_2	0.54	1.38	0	0.37	1.41	0	0.06	0.2	0
	Al_2O_3	34.03	37.49	31.52	33.43	36.53	28.29	34.05	35.66	31.76
	FeO	2.64	6.03	1.42	1.68	2.85	0.49	1.85	2.97	1.08
	MnO	0.05	0.15	0	0.02	0.09	0	0.02	0.06	0
	MgO	0.62	1.12	0.29	0.73	1.26	0.22	1.26	1.88	0.85
	CaO	0.14	0.89	0	0.16	0.97	0	0.04	0.24	0
	Na_2O	0.56	1.26	0.1	0.3	1.65	0.02	0.29	0.48	0.05
	K_2O	9.29	10.23	7.37	9.58	11.08	6.08	10.43	10.99	9.53
	H_2O	4.5	4.62	4.38	4.52	4.69	4.36	4.58	4.65	4.49
	Total	99.48			99.31			101.27		
Cations to 12 O, OH	Si	3.14	3.34	3.03	3.22	3.63	3.04	3.19	3.35	3.12
	Al	0.86	0.97	0.66	0.78	0.96	0.37	0.81	0.88	0.65
	Al	1.81	1.95	1.73	1.83	1.94	1.75	1.81	1.88	1.73
	Ti	0.03	0.07	0	0.02	0.07	0	0	0.01	0
	Cr	0	0	0	0	0	0	0	0	0
	Fe^{2+}	0.15	0.34	0.08	0.09	0.16	0.03	0.1	0.16	0.06
	Mn	0	0.01	0	0	0.01	0	0	0	0
	Mg	0.06	0.11	0.03	0.07	0.13	0.02	0.12	0.19	0.08
	Ca	0.01	0.06	0	0.01	0.07	0	0	0.02	0
	Na	0.07	0.16	0.01	0.04	0.21	0	0.04	0.06	0.01
	K	0.79	0.87	0.62	0.81	0.96	0.51	0.87	0.93	0.78

Table 4
Summary of biotite EPMA analyses from Chepelare metapelites.

		2-1-10						47-1-11			3-1-10					
		Matrix ($n = 38$)			Inclusion ($n = 6$)			Matrix ($n = 4$)			Matrix ($n = 39$)			Inclusion ($n = 18$)		
		Avg	Max	Min	Avg	Max	Min	Avg	Max	Min	Avg	Max	Min	Avg	Max	Min
Oxide wt%	SiO_2	35.86	36.89	32.86	36.22	37.06	35.28	35.9	36.06	35.8	34.66	35.74	33.62	35.06	37.86	34.38
	TiO_2	3.82	4.61	2.59	3.31	4.49	2.71	2.37	2.45	2.3	2.15	3.02	1.4	2.07	2.44	1.56
	Al_2O_3	17.95	19.26	16.11	18.33	18.63	18.14	17.89	18.24	17.7	20.18	22.19	19.16	20.61	24.08	19.74
	Cr_2O_3	0.02	0.06	0	0.02	0.05	0	–	–	–	0.02	0.06	0	0.02	0.05	0
	FeO	17.12	19.59	14.74	17.12	18.44	16.32	16.54	16.8	16.32	23.05	24.64	19.82	21.72	23.63	17.69
	MnO	0.03	0.08	0	0.03	0.06	0	0.03	0.04	0.01	0.08	0.33	0.01	0.08	0.13	0.02
	MgO	11.37	12.52	10.28	11.96	12.24	11.6	12.27	12.41	12.17	7.11	7.55	6.13	7.73	9.04	5.81
	CaO	0.07	1.83	0	0	0.01	0	−0.01	0.01	−0.03	0.03	0.66	0	0.03	0.06	0
	Na_2O	0.15	0.29	0.08	0.18	0.22	0.14	0.25	0.27	0.22	0.27	0.32	0.2	0.29	0.34	0.2
	K_2O	7.99	9.23	6.24	7.85	8.32	7.27	8.71	8.8	8.52	8.76	9.06	7.7	8.85	9.04	8.66
	H_2O	3.96	4.04	3.72	4	4.03	3.96	3.95	3.96	3.94	3.93	3.98	3.86	3.96	4.09	3.91
	Total	98.41	100.45	92.75	99.08	99.73	98.27	97.91	98.25	97.65	100.23	101.55	98.09	100.42	101.09	99.11
Cations to 12 O, OH	Si	2.68	2.72	2.6	2.68	2.71	2.64	2.72	2.73	2.72	2.65	2.71	2.58	2.65	2.77	2.63
	Al^{iv}	1.32	1.4	1.28	1.32	1.36	1.29	1.28	1.28	1.27	1.35	1.42	1.29	1.35	1.37	1.23
	Al^{vi}	0.26	0.33	0.17	0.27	0.29	0.24	0.33	0.35	0.31	0.46	0.7	0.4	0.49	0.85	0.42
	Ti	0.21	0.26	0.15	0.18	0.25	0.15	0.14	0.14	0.13	0.12	0.17	0.08	0.12	0.14	0.09
	Cr	0	0	0	0	0	0	0	0	0	0	0	0	0	0	0
	Fe^{2+}	1.07	1.25	0.91	1.06	1.15	1	1.05	1.06	1.04	1.47	1.57	1.26	1.38	1.51	1.08
	Mn	0	0.01	0	0	0	0	0	0	0	0.01	0.02	0	0	0.01	0
	Mg	1.27	1.38	1.15	1.32	1.36	1.27	1.39	1.4	1.38	0.81	0.86	0.7	0.87	1.02	0.63
	Ca	0.01	0.15	0	0	0	0	0	0	0	0	0.05	0	0	0	0
	Na	0.02	0.04	0.01	0.03	0.03	0.02	0.04	0.04	0.03	0.04	0.05	0.03	0.04	0.05	0.03
	K	0.77	0.88	0.6	0.75	0.79	0.7	0.84	0.85	0.82	0.85	0.88	0.75	0.85	0.87	0.83
	OH	1.99	2	1.97	1.99	1.99	1.99	2	2	2	2	2	2	2	2	2
	Mg#	54	60	48	55	56	54	57	57	56	35	37	32	39	44	35

temperatures calculated from rutile inclusions and matrix rutile in either sample.

4.2.2.2. Garnet–biotite thermometry. The garnet–biotite Fe–Mg exchange thermometer was also used to constrain metamorphic temperatures. The relationship between temperature and Fe–Mg content of coexisting garnet and biotite was first recognized by Kretz (1959), and the first experimental thermometer was published by Ferry and Spear (1978) based on the equation: almandine + phlogopite = pyrope + annite. Subsequent work has refined this thermometer by expanding the

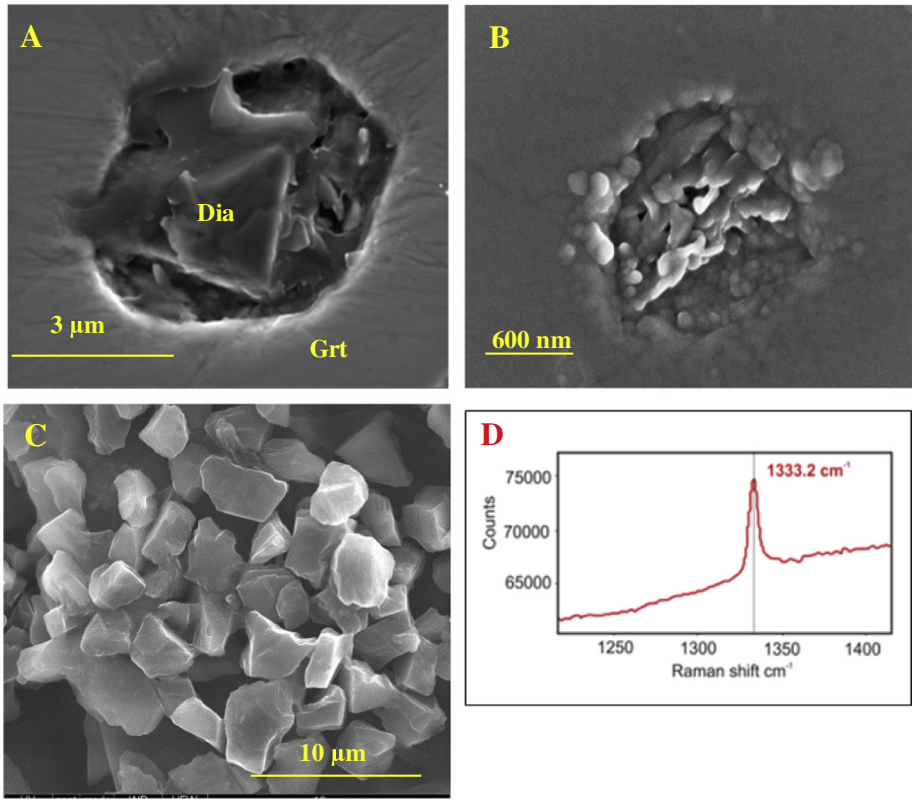

Fig. 5. (A) SEM image of microdiamond inclusion from sample 3-1-10. (B) SEM image of carbon inclusion that fluoresced under CL light from sample 3-1-10. (C) SEM image of diamond polishing paste. (D) Laser Raman spectra from microdiamond.

effective temperature range of the thermometer and taking into account the effect of elements such as Ti and Al^{VI} in biotite and Ca and Mn in garnet. Accordingly, a number of different calibrations now exist for this thermometer and have been used to calculate temperatures. Temperatures have been calculated at pressures of both 1 and 4 GPa for samples 25-1-10 and 3-1-10 and are presented in the supplementary material. The calibration by Bhattacharya et al. (1992) has been shown to be less affected by pressure variations than other calibrations and is therefore the favoured for this study.

Analyses of garnets rims paired with matrix biotite calculated at 4 GPa in sample 25-1-10 yield temperatures between 630 and 740 °C, with an average of 671 °C. In sample 3-1-10, the average from the same setting is 608 °C, with a narrower range of 563–628 °C. In both samples, calculations using inclusions of biotite within garnet yield lower temperatures than garnet rim analyses paired with matrix biotite, likely due to diffusion between biotite inclusions and adjacent garnets.

Calculated temperatures using garnet rim-biotite pairs are likely blocking temperatures, owing to the effects of retrograde diffusion at the garnet rims. Accordingly, the average core composition of the garnet and matrix biotite not in contact with garnet was used to calculate temperatures for sample 3-1-10. This calculation yielded higher temperatures (average = 684 °C), closer to the range of values determined using the Zr-in-rutile thermometer. This calculation was not possible in sample 25-1-10, owing to the lack of matrix biotite in equilibrium with garnet.

4.2.3. Geobarometry

The diverse mineral assemblage and uncertainty surrounding coexisting mineral phases makes the applicability of continuous net transfer equilibria barometers, such as GASP (garnet–Al_2SiO_5-quartz-plagioclase) and GRAIL (garnet–rutile–Al_2SiO_5–ilmenite–quartz), to the Chepelare garnet–kyanite metapelites questionable. Previous studies have reported pressures of 1.2-1.4 GPa for Chepelare metapelite samples (Georgieva, et al., 2007), significantly below the peak pressures suggested by the microdiamond inclusion.

The Si content of phengite has been shown to increase with increasing pressure (Konrad-Schmolke et al., 2011; Massonne and Szpurka, 1997), although absolute values are dependent on both the composition of the sample and the equilibrium assemblage. Models produced for the assemblage, garnet + kyanite + phengite + quartz (the peak assemblage inferred from petrological observations), suggest that phengite with Si a/fu >3.5 formed at pressures >30 kbar (Massonne and Szpurka, 1997). Accordingly, the Si content of phengite in sample 3-1-10 (up to 3.63 a/fu) could indicate UHP conditions. The Ti content of phengite has been proposed as a single element barometer suitable for samples that experienced UHP conditions based on the equilibrium $^{VI}Ti^{IV}Al$–$^{VI}Al^{IV}Si$ exchange in muscovite and phengite occurring in equilibrium with rutile and quartz/coesite (Auzanneau et al., 2010). The pressure dependence of this exchange has since been questioned (Chambers and Kohn, 2012), and results of this study indicate that the most phengitic muscovite crystals do not contain enough Ti to be suitable for geobarometry using the Auzanneau et al. (2010) calibration.

4.3. Garnet geochronology

4.3.1. Age of garnet separates

The isotopic compositions of five bulk garnet separates are presented in Table 5. Multiple repeat analyses were conducted on samples 47-1-11 and 3-1-10, the diamond-bearing sample. With the exception of sample 47-1-11, all samples yielded high $^{147}Sm/^{144}Nd$ (>1.0) and low Nd concentrations (<0.5 ppm), indicative of the successful removal of contaminating inclusions during partial dissolution (e.g. Baxter and Scherer, 2013). Each garnet analysis was paired with its respective whole rock to determine a two-point isochron age. All calculated garnet ages are Late Cretaceous, with calculated values ranging from 70.3 to 99.6 Ma (Table 6). All isochron ages were calculated using the Isoplot Program (Ludwig, 2003). For age error determination, we used the poorer (higher) of the reported internal analytical precision for each analysis (Table 5) or the external precision of the standard. Since multiple garnet separates were processed for samples 3-1-10 and 47-1-11, multipoint isochrons were also calculated for those samples yielding more robust age constraints of 70.5 ± 2.7 (MSWD = 0.07) and 92.7 ± 7.1 (MSWD = 2.8) (Fig. 6).

4.3.2. Age of single zoned garnet crystal

Isotopic data from the five drilled garnet zones in sample 27-1-10 are shown in Fig. 7 and Table 7, and a summary of calculated ages are presented in Table 8. Included in these data are the whole rock encapsulating the garnet, the original "bulk" garnet analysis, as well as two analyses of intentionally uncleaned garnet powders derived from zones 1 and 5. Note that the two uncleaned garnet powders fall significantly off of any garnet–WR isochron, reflecting an inherited component within garnet inclusions. Such inclusion-contaminated garnets should not be included in any garnet isochron. Note also the difference between the uncleaned "garnet" powders and the acid-cleaned garnets with much higher $^{147}Sm/^{144}Nd$ and much lower [Nd], indicative of the success and importance of inclusion removal.

Among the acid-cleaned garnet zones, zone 1 (the core) stands as a clear outlier well below (i.e. apparently *younger* than) any garnet–WR isochron, especially as the core should be older than the rim. Reasons for this outlier zone 1 data will be addressed below, but if it is removed from consideration, the remaining analyses (Zones, 2,3,4,5, and bulk garnet; Fig. 7b) fall on a near isochron with the whole rock yielding 87 ± 12 Ma (MSWD = 3). Closer inspection reveals that zone 2 is slightly below (younger) than the isochron, perhaps for reasons similar to zone 1. Eliminating zone 2 reveals a statistically robust isochron (e.g. Wendt and Carl, 1991), including the WR, zones 3, 4, 5, and the bulk garnet of 83.6 ± 2.9 (MSWD = 1.9). For the present purpose, we consider the 83.6 ± 2.9-Ma age to be an accurate measure of the majority of garnet growth spanning at least zones 3,4, and 5. This indicates that

Table 5
Sm–Nd isotope data collected for both whole rock samples and garnet separates. BG: bulk garnet separate; WR: whole rock.

Sample	Sm (ppm)	Nd (ppm)	ng Nd loaded	$^{147}Sm/^{144}Nd$	±2 SE (ppm)	$^{143}Nd/^{144}Nd$	±2 SE (ppm)
38-1-11 Grt	1.026	0.367	13.1	1.690875	0.000389	0.512771	0.00003
27-1-10 Grt	1.749	0.498	6.7	2.122316	0.000788	0.51315	0.000079
3-1-10 Grt 1	0.457	0.208	4.4	1.331532	0.000306	0.512441	0.000017
3-1-10 Grt 2	0.537	0.309	9.6	1.049758	0.000085	0.512314	0.000015
2-1-11 Grt	0.837	0.375	10.3	1.351216	0.00043	0.512598	0.000013
47-1-11 Grt 1	1.006	1.005	18.9	0.605892	0.000207	0.512212	0.000012
47-1-11 Grt 2	0.792	1.065	16.9	0.449974	0.00005	0.512135	0.000008
38-1-11 WR	17.392	94.458	72.99	0.111374	0.000026	0.511938	0.000007
27-1-10 WR	10.822	70.294	69.36	0.093124	0.000021	0.511965	0.000006
3-1-10 WR	8.304	45.382	49.21	0.110683	0.000012	0.511879	0.000008
2-1-11 WR	11.95	64.308	78.35	0.112403	0.000026	0.511871	0.000014
47-1-11 WR	2.538	11.294	48.4	0.135933	0.000031	0.51193	0.000008

Table 6
Summary of ages calculated for garnet separate–whole rock pairs. Ages highlighted in bold are the preferred ages calculated for samples.

Sample	Age (Ma)	Error (Ma)	MSWD
38-1-11 Grt	**80.6**	**3.2**	N/A
27-1-10 Grt	89.3	5.9	N/A
3-1-10 Grt 1	70.4	2.9	N/A
3-1-10 Grt 2	70.8	3.6	N/A
2-1-11 Grt	**89.7**	**2.7**	N/A
47-1-11 Grt 1	91.7	7.2	N/A
47-1-11 Grt 2	100	11	N/A
3-1-10 MULTI-PT	**70.5**	**2.7**	**0.067**
47-1-11 MULTI-PT	**92.7**	**7.1**	**2.8**

the majority of the garnet in this sample grew rapidly at this time (~83.6Ma).

5. Discussion

In this work, we have presented the first discovery of microdiamond inclusions from the central (Bulgarian) portion of the RM, which provides further evidence for widespread UHP conditions in this region. The petrological insights and the thermobarometric estimates suggest that the kyanite–garnet schists from the VF melange units around the town of Chepelare have experienced pressures in excess of 4 GPa. This new discovery complements the well-studied microdiamond localities from the Greek part of the RM, and Sm–Nd dating performed in this study indicates a Late Cretaceous ages of the UHP metamorphism.

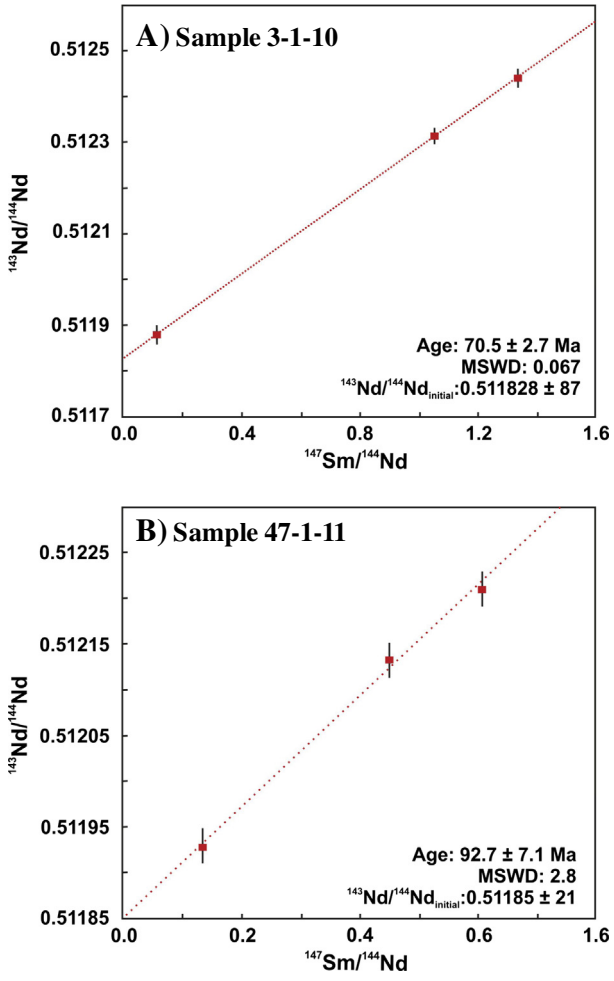

Fig. 6. (A) Three-point isochron calculated for sample 3-1-10, the diamond-bearing sample from Chepelare, Central Rhodope Mountains. (B) Three-point isochron calculated for sample 47-1-11, the phaneritic "museum" sample, also from Chepelare.

5.1. Interpretation of the Late Cretaceous (UHP) metamorphic ages

In light of the high temperatures experienced by the metapelitic samples in the vicinity of Chepelare, as calculated by Zr in rutile thermometry, and the variable degrees of partial melting observed (Cherneva and Georgieva, 2005), the potential for thermal resetting of the Sm–Nd system in the kyanite–garnet schist samples must be considered before discussing the implications of a Late Cretaceous UHP metamorphic event.

Little variation is seen in calculated Zr in rutile temperatures, irrespective of petrographic location. All are consistently in the range of 775–800 °C, and as such, it is not possible to link different rutile temperatures with periods of garnet growth. Owing to the known complex subduction–exhumation history associated with these samples, it is difficult to relate with any certainty current textural relationships and the UHP event. The calculated Zr in rutile temperatures for rutile crystals included within garnet does however suggest that the garnet experienced temperatures in among those proposed for the closure of the Sm–Nd system (Smit et al., 2013). Thermal re-equilibration of the garnet chemistry could explain the observed spread in ages (20 Ma) for the five aggregate garnet samples. However, thermal re-equilibration is not supported due to the preservation of prograde Mn and Ca growth zones in samples–elements that should be mobile above the closure temperature of the Sm–Nd system (Carlson, 2012; Mezger et al., 1992). If the garnet ages had been reset, correlation between the measured Sm–Nd ages and the garnet size would be expected, owing to the diffusion behaviour of REE in garnet (Duth and Hand, 2010). This relationship is not seen, and dating of individual zones from the large garnet crystal (sample 27-1-10) yields broadly similar ages to all of the other samples. As such, the calculated ages are interpreted to represent the timing of garnet growth rather than a thermal resetting event or cooling.

The spread in calculated ages could be related to the partial dissolution cleansing technique used to clean the garnet crystals prior to full dissolution. While it is possible that the spread in ages is an artifact of remaining inclusions influencing the garnet analysis, that effect is unlikely to be significant in well-cleaned garnet samples with Sm/Nd >1.0 (e.g. Baxter and Scherer, 2013) and thus only potentially impacts sample 47-1-11. More likely, the recorded ages are accurate and reflect growth in the different rocks of the study area over a period of approximately 20 Ma. This agrees with the large spread in ages of the calc-alkaline magmatic rocks found in the Sredna Gora magmatic zone to the north of the RM associated with the northward subduction of the Neotethys ocean. Subduction-related deposits (including Cu-Au mineralizations) in this area have ages raging between 92 and 69 Ma, with a general younging from N–S associated with slab retreat (Georgiev et al., 2012; Peytcheva et al., 2008; Von Quadt et al., 2005).

Although clearly anomalous, the apparently younger age for the garnet core (zone 1, and perhaps part of zone 2) merits further discussion. Diffusional resetting of an older core age before subsequent growth is unlikely to have been a factor given the preservation of clear Mn zonation in the dated garnet (Fig. 4). Divalent cation diffusivity is faster than REE diffusivity in garnet, so preservation of the former indicates preservation of the latter (Carlson, 2012). Often, artificially young ages in Sm/Nd garnet geochronology are the result of incomplete removal of Nd-rich inclusions during partial dissolution. As the two inner zones underwent the same partial dissolution procedure as the three outer zones and all 5 zones have similarly high $^{147}Sm/^{144}Nd$ values and low [Nd] ppm, this explanation seems unlikely. A resistant retrograde mineral unique to the garnet core, such as allanite, could alternatively explain the anomaly, but no suitable inclusion candidate has been identified in garnet cores from the thin section of this sample. Resorption and recrystallization of the core during retrograde metamorphism,

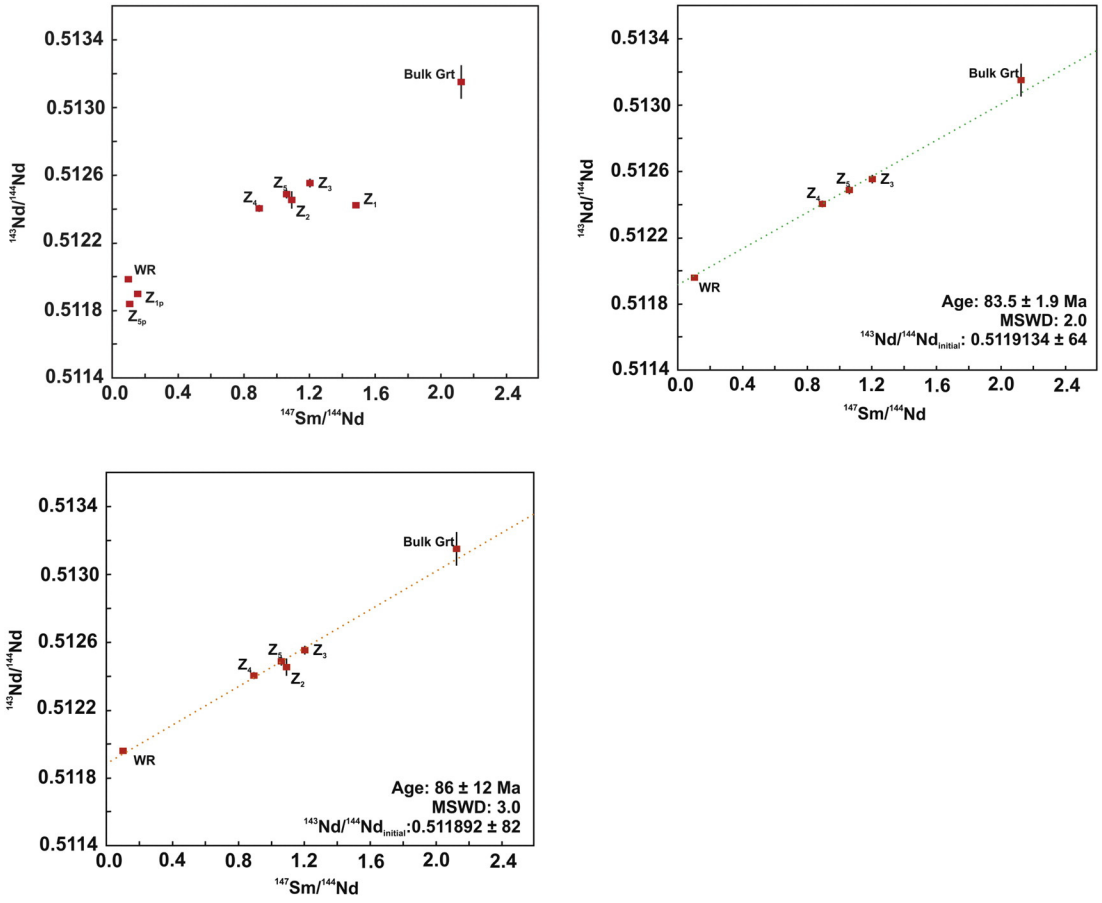

Fig. 7. TL: Overview of all isotope data collected from the zoned garnet crystal. Z1P and Z5P: Uncleaned powders of garnet zones Z1 and Z5, respectively. TR: five-point isochron calculated using the values for whole rock (WR), bulk garnet (BG), and garnet zones Z3, Z4, and Z5. BL: six-point isochron calculated using the WR, BG, and Z2, Z3, Z4, and Z5 values.

akin to formation of atoll garnets, would explain the age profile but is not reflected in thin section textures or in keeping with the prograde zonation generally preserved in garnet crystals.

A recent study by Gatewood, et al. (2015) also reported garnet cores apparently younger than rim ages in certain porphyroblasts from the same rock and attributed the age difference to local matrix heterogeneity, possibly including open system matrix evolution during/after garnet growth. A shift in the whole rock $^{143}Nd/^{144}Nd$ or $^{147}Sm/^{144}Nd$ that occurred between growth of the core and the outer zones could explain an anomalously young core age since pairing the current volume-averaged whole rock with the garnet core would violate isochron assumptions. It is possible that the core overgrew an area of isotopically different matrix, not at all unlikely in a layered heterogeneous sedimentary protolith, before more intense metamorphism served to homogenize matrix composition at the mm to cm scale as later garnet continued to grow. Alternatively, the partial melting and subsequent open system behavior experienced by the Chepelare metapelites could facilitate such a shift in matrix Sm/Nd, assuming melting and new garnet growth occurred simultaneously. The core (zone 1) may have initiated growth at some earlier (older) time than the outer zones but that age record appears to have been compromised by subsequent open system processes. The majority of garnet growth (zones 3, 4, and 5) in this samples occurred at 83.6 ± 2.9 Ma.

Despite being widespread across the RM, Late Cretaceous ages have not previously been reported from metamorphic units in the Central Rhodope Mountains (Bulgaria). The only exception was from zircon rims from Cenozoic pegmatite bodies (Bosse et al., 2009). One interpretation of the bulk garnet separate ages could be that the Late Cretaceous timing represent some kind of an averaging of the ~150 Ma and ~40 Ma domains recorded in the monazite record (Bosse et al., 2010; Didier et al., 2014). However, the dating of individual zones from within a garnet crystal in this study demonstrates that this is not possible given

Table 7
Sm–Nd isotope data for single zoned garnet crystal from Chepelare region metapelites. Z1–Z5 correspond to zones 1–5 defined in Fig. 4, P1 and P5: Garnet powders collected during hand-crushing of zones 1 and 5.

Sample	Sm (ppm)	Nd (ppm)	ng Nd loaded	$^{147}Sm/^{144}Nd$	±2 SE (ppm)	$^{143}Nd/^{144}Nd$	±2 SE (ppm)
27-1-10 Z1	1.184	0.483	6.52	1.482306	0.000547	0.512406	0.000011
27-1-10 Z3	0.818	0.412	3.28	1.201346	0.000313	0.512556	0.000021
27-1-10 Z4	0.927	0.629	10.22	0.891774	0.000307	0.512405	0.000017
27-1-10 Z5	1.046	0.598	3.34	1.058207	0.000243	0.51249	0.000021
27-1-10 WR	10.822	70.294	69.36	0.093124	0.000021	0.511965	0.000006
27-1-10 P1	3.632	14.675	5.12	0.149733	0.000042	0.511899	0.000013
27-1-10 P5	36.791	220.6	158.4	0.100879	0.000023	0.511846	0.000005

Table 8
Summary of ages calculated for individual zones and multi zone isochrons for sample 27-1-10. The age highlighted in bold is the preferred age of this sample.

Sample	Age (Ma)	Error (Ma)	MSWD
27-1-10 Z1	48.5	2.4	N/A
27-1-10 Z2	75	6.9	N/A
27-1-10 Z3	81.5	3.6	N/A
27-1-10 Z4	84.2	4.4	N/A
27-1-10 Z5	83.2	4.1	N/A
27-1-10 WR,blk, Z2-5	87	12	3
27-1-10 WR,blk, Z3-5	**83.6**	**2.9**	**1.9**

that most of the garnet volume (zones 3, 4, 5) grew rapidly at 83.6 ± 2.9 Ma. The garnets in this study reveal for the first time a Late Cretaceous UHP metamorphic event in the Central Rhodope Mountains.

Although rare in the vicinity of Chepelare (and anywhere within the Central Rhodopes Mountains), Late Cretaceous metamorphic ages have been widely reported from other parts of the RM in HP zircon rims from both garnet-rich mafic rocks and their surrounding orthogneiss in the diamond-containing Kimi Complex in Greece (Liati et al., 2002; Liati et al., 2011). The robust nature of zircon means that grains may survive multiple metamorphic events and be recycled in more recent processes than their preserved "age" might suggest (Lee et al., 1997). This is demonstrated by age zonation in individual zircon grains. In recent years, this has been combated with trace element analysis, which can distinguish magmatic and metamorphic zones within individual crystals. Zircon that formed under high-pressure conditions has a flatter REE profile and a smaller negative Eu anomaly than their magmatic counterparts (Rubatto, 2002). Zircons from all four of the proposed UHP age-groups (ca. 150 Ma, ca. 73 Ma, ca. 51 Ma, and ca. 42 Ma) have these HP indicators, and as such constraining the UHP event solely based on zircon geochronology remains problematic (Liati et al., 2011).

With all microdiamond discoveries from the RM occurring as inclusions within garnet alongside exsolution textures indicative of HP conditions, Liati et al. (2011) questioned how this evidence could have survived numerous (3?) subsequent HP/HT metamorphic events if the UHP event was Jurassic, or even older. A Late Cretaceous age for UHP metamorphism eliminates this problem. As such, the new Sm–Nd garnet ages from Chepelare reported in this study compliments well the existing (largely U–Pb zircon) geochronological data set for the RM (Fig. 8), and acts as a new link between the Central and the Eastern Rhodope Mountains.

5.2. Tectonic implications of a Late Cretaceous age of the UHP metamorphism in the Rhodopes

The restriction of upper allochthon (VF/UHP) units in the Bulgarian and Greek Central Rhodope Mountains to a melange zone along the Chepelare and Nestos Shear Zones has been used to place constraints on the geodynamic evolution of the RM. The Nestos Shear Zone was originally believed to mark a suture between the Variscan granite of the lower high-grade basement units and the VF. In this scenario, UHP units were believed to form in a Jurassic subduction zone, with samples experiencing a prolonged single subduction–exhumation cycle, with accretion ages ranging from the Jurassic through Eocene (Krenn et al., 2010; Ricou et al., 1998; Turpaud and Reischmann, 2010). This model is, however, difficult to reconcile with the current geochronological data from the RM. There is no way to explain a pulsed metamorphic history with a Late Cretaceous UHP metamorphic event.

Alternatively, the Nestos Shear Zone may represent a stretching fault at the base of a collapsing orogenic wedge. This model, suggested by Nagel et al. (2011) is based on the lower high-grade basement unit occupying an external position in the Hellenide nappe stack, exposed beneath an orogenic scale out of sequence thrust (the Nestos Shear Zone), which extends underneath the Cretaceous nappe pile west of the RM, reaching the surface between the Pindos Zone and the external Hellenides. In this scenario, UHP metamorphism in the RM is proposed to be the result of southward subduction of the Meliata and Malica oceanic crust during the Jurassic, prior to opening of the Vardar Ocean and the northward (Cretaceous) subduction under the Eurasian margin. Evidence for this Jurassic south dipping convergent plate margin and associated exhumation of metamorphic rocks is preserved in the low-grade Mesozoic units of the Circum Rhodope belt (Bonev et al., 2010). In this model, during subduction of the Vardar Ocean, only units from the middle and lower allochthons were involved in the Cretaceous–Eocene northward-dipping subduction event—the UHP units of the upper allochthon were already exhumed and emplaced in the overriding plate. If correct, the Kimi complex currently represents the true stratigraphic position of UHP units in the RM, and the position of UHP metapelites in the Chepelare and Nestos Shear Zones is the result of Late Cretaceous slab rollback, which facilitated orogenic wedge collapse and Cenozoic faulting. Reported Eocene-related HP metamorphism from middle allochthon (not UHP VF) eclogites in the Cetntral Rhodope Mountains near Chepelare (Kirchenbaur et al., 2012) is used as key evidence to support this theory.

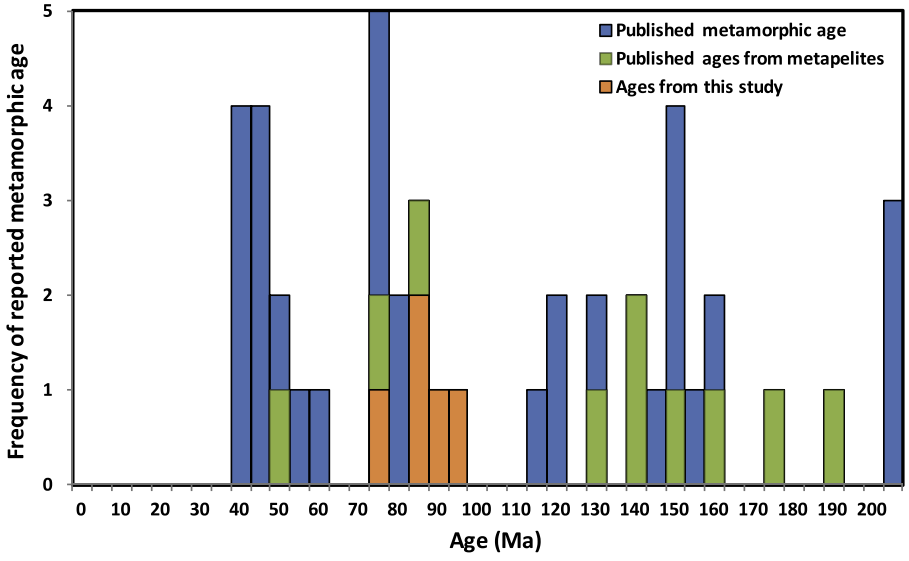

Fig. 8. Histogram of published metamorphic ages (Table 1) from across the Rhodope Massif. Green bars represent ages dates obtained from metapelites, orange bars represent new ages presented in this study. Bin size: 5 Ma. (For interpretation of the references to color in this figure legend, the reader is referred to the web version of this article.)

Although this model accounts for a pulsed metamorphic record across the RM, it is not in keeping with the age results we report here. Irrespective of whether the Late Cretaceous age is recording garnet growth or a thermal resetting event, the Late Cretaceous age must be the result of the Northward subduction of the Vardar/Paleothethys Ocean. This age is therefore not compatible with the subduction and exhumation of the VF/Upper Allochthon during the Jurassic prior to a quiescent period in the overriding plate through the Cretaceous subduction event. In addition, the genetic link between UHP units and the southward dipping Jurassic subduction event recorded in Mesozoic schists of the Circum Rhodope belt is based solely on U–Pb zircon geochronology, which has the added complication of possible inheritance. No Jurassic Sm–Nd or Lu–Hf garnet ages have been recorded in (U)HP units anywhere across the RM.

In the vicinity of Chepelare Eocene ages are not simply restricted to ecogite boudins (Kirchenbaur et al., 2012) but have been reported from matrix monazite crystals in metapelites (Bosse et al., 2010; Didier et al., 2014), pegmatites in the host gneiss (Bosse et al., 2009), and discordant leucosomes in the Arda 2 gniess (Cherneva and Georgieva, 2005). The recognition of a common Eocene metamorphic event in units proposed to belong to both the middle and upper allochthon, alongside the absence of evidence for Eocene metamorphism in the garnets of this

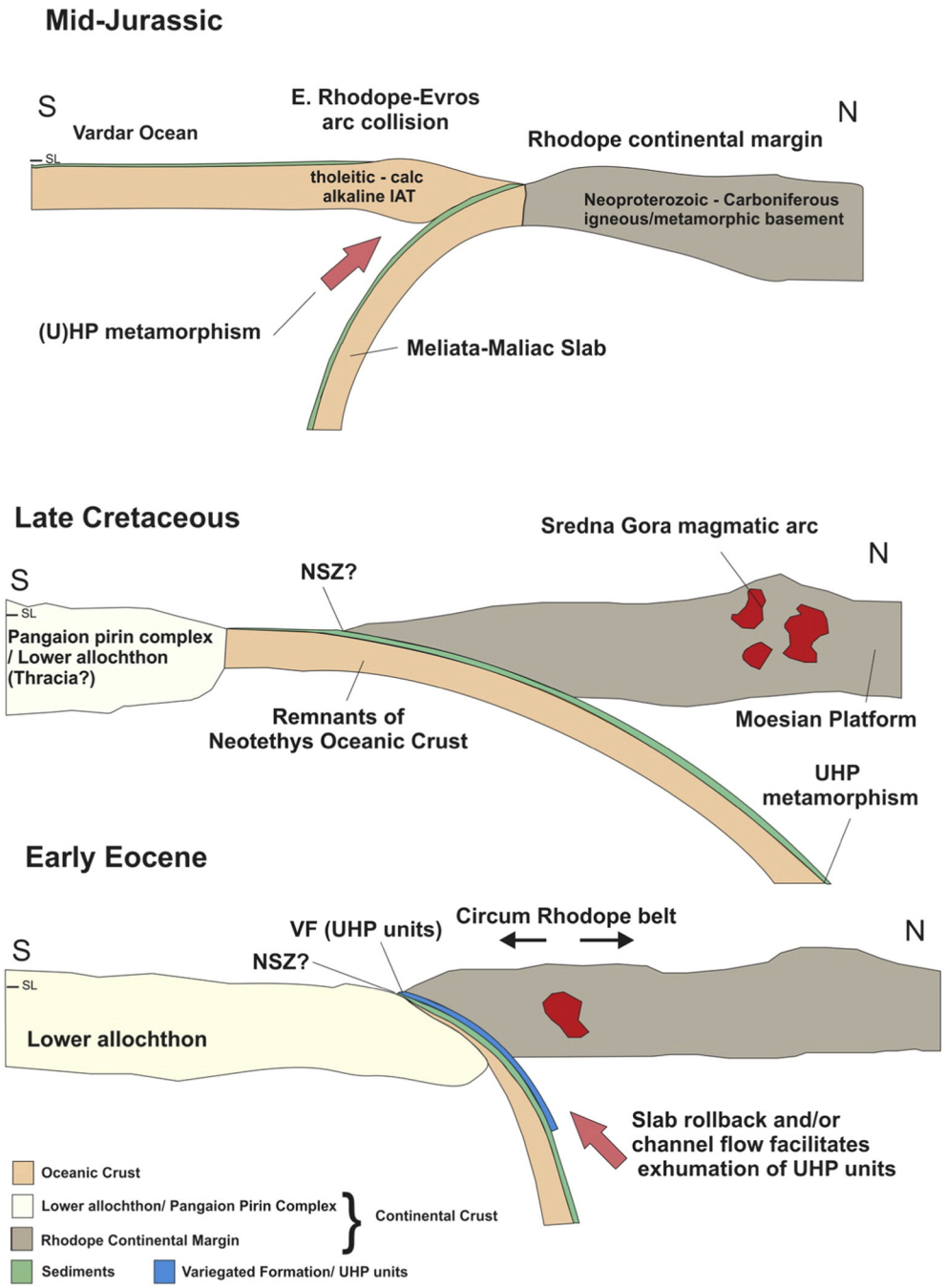

Fig. 9. Simplified tectonic model for the evolution of the Rhodope Massif incorporating our new metamorphic age results. This model accommodates a southward dipping Cretaceous subduction zone (which has been documented in the Circum Rhodope belt; Bonev et al., 2011) prior to a Late Cretaceous northward-dipping subduction zone that led to the formation of the Sredna Gora magmatic arc and the UHP metamorphic units found throughout the Variegated Formation of the Rhodope Massif. Final exhumation of samples occurred in the Early Eocene as a result of slab rollback from the subduction of continental crust or channel flow. It remains unclear whether the Rhodope Massif has experienced multiple periods of UHP metamorphism or if the Late Cretaceous event suggested by this study is the only UHP metamorphic event.

study, indicates juxtaposition of all of these units prior to an Eocene metamorphic event, with temperatures not high enough to rest the Sm–Nd ages of the garnet crystals. This effectively eliminates the age populations at 42 and 51 Ma (Fig. 8) as possibilities for the age of the UHP event.

The increasing evidence for a southern-dipping subduction zone during the Late Jurassic to Early Cretaceous associated with the closure of the Meliata–Maliac Ocean (Bonev and Stampfli, 2008; Bonev et al., 2010) agrees with a Late Cretaceous UHP metamorphic event. A scenario, as first proposed by Liati et al. (2011), involving the amalgamation of a series of different microcontinents is envisioned. This would cohesively explain the pulsed nature of ages preserved in the metamorphic record and the Late Cretaceous UHP ages reported in this study.

In this scenario, the UHP units formed part of the subducting slab dipping North in the Cretaceous, agreeing with models proposed by Turpaud and Reischmann (2010) and Burg (2012). A Late Cretaceous UHP metamorphic event also allows sufficient time for a complete subduction–exhumation cycle related to a prior southward dipping Jurassic/Early Cretaceous subduction as suggested by Bonev et al. (2010). As such, a hybrid of the two existing geodynamic models is envisioned (Fig. 9).

The new model allows for a regional southward dipping subduction zone in the Mid-Jurassic to Early Cretaceous from the Circum Rhodope belt (Bonev and Stampfli, 2011; Bonev et al., 2010). Zircon geochronologic studies indicate that this subduction event led to at least HP metamorphism (Liati et al., 2011). Subsequently, a subduction reversal event occurred. This regional northward-dipping subduction is widely documented on the territory of Bulgaria and led to the formation of the Sredna Gora mountain range and magmatic arc (Georgiev et al., 2012; Peytcheva et al., 2008; Von Quadt et al., 2005). Results of this study are among the first to indicate that the northward-dipping Cretaceous subduction zone was indeed the source of the regional UHP metamorphism in the RM of the SE Europe.

No existing model for exhumation of UHP units is able to account for a long, protracted exhumation process as suggested by many proponents of a Jurassic UHP metamorphic event (Burg, 2012; Krenn et al., 2010; Turpaud and Reischmann, 2010). The Eocene HP metamorphic event (Kirchenbaur et al., 2012; Nagel et al., 2011) can be explained through either exhumation via subduction channel flow or slab rollback, both of which can account for the restriction of UHP conditions to metapelitic units within the VF and the widespread of ages observed across the RM. Slab rollback is consistent with the Late Cretaceous UHP event documented in this study, with the UHP units forming in a northward-dipping slabs. North to south younging of Late Cretaceous magmatism in the Sredna Gora volcanic arc can be explained by the subduction of one of the many buoyant Tethyan microcontinents (Stampfli and Borel, 2002), and the resultant slab steepening due to the influx of buoyant material which will slow the subduction rate. Eocene metamorphic ages can be related to the subsequent regional extension related to the formation of the metamorphic core complexes that dominate the geology of the lower allochthon.

The mixing of units with contrasting P-T-t histories in both the Nestos and the Chepelare shear zones and the restriction of UHP localities to localized areas also fit well with computational models for both channel flow (Hacker and Gerya, 2013) and plunger expulsion (Warren, 2013). These mechanisms are compatible with a Jurassic or a Late Cretaceous UHP event, although the complex post-peak metamorphic history likely inhibits further deductions about the exhumation history of the UHP rocks.

Further work is required to address both the extent of heterogeneity within the middle allochthon and the magnitude of the Eocene metamorphic event in order to fully understand the Cenozoic evolution of the RM. It remains unclear whether this is a continuation of the same Late Cretaceous (U)HP subduction zone or a separate HP subduction–exhumation event postdating the UHP metamorphism.

6. Conclusion

This study provides compelling evidence for a new UHP locality in the central part of the RM in Bulgaria. This new discovery extends the current UHP region of SE Europe and acts as a missing link between discoveries in the Eastern and Western parts of the massif, while raising questions about stratigraphic correlations drawn across the massif, the subdivision of basement units, and the timing of the peak metamorphic event. Sm–Nd garnet geochronology on diamondiferous metapelitic samples suggests a Late Cretaceous UHP metamorphic event, which is significantly younger than the Jurassic UHP event currently proposed by monazite and zircon geochronology but in agreement with HP metamorphic conditions recorded in zircons across the Eastern Rhodope Mountains. A Late Cretaceous age indicates that the upper allochthon formed part of the Vardar Ocean, which was subducting northward under the Moesian Platform and that the RM has had a varied tectonic history with multiple subduction–exhumation events spanning the Jurassic to Eocene.

Acknowledgments

Alicia Cruz Aribe and Matthias Konrad-Schmolke are thanked for their helpful reviews. Bruce Yardley, Milena Georgieva, Nikolay Bonev, Bob Cliff, and the Leeds University High Temperature Geochemistry Research Group are all thanked for many fruitful discussions. Richard Walshaw and Eric Condliffe from the Leeds Electron Microscopy and Spectroscopy centre are thanked for their help with the SEM and EPMA mineral chemistry data collection. Denise Honn and Besim Dragovic are thanked for their assistance with the Sm–Nd measurements in the TIMS lab at Boston University. Sv. Petrussenko from the National Museum of Natural History, Bulgaria, is thanked for the donation of samples and the advice given during fieldwork. This work was funded by a NERC doctoral training grant and by the William George Fearnsides grant of the Geological Society of London.

EFB is grateful for support from NSF Grant EAR-0948308. The BU TIMS Facility was supported by NSF Grants EAR-0521266 and EAR-0949390.

Appendix A. Supplementary data

Supplementary data to this article can be found online at http://dx.doi.org/10.1016/j.lithos.2016.01.002.

References

Auzanneau, E., Schmidt, M.W., Vielzeuf, D., Connolly, J.A.D., 2010. Titanium in phengite: a geobarometer for high temperature eclogites. Contributions to Mineralogy and Petrology 159, 1–24.

Bauer, C., Rubatto, D., Krenn, K., Proyer, A., Hoinkes, G., 2007. A zircon study from the Rhodope metamorphic complex, N-Greece: time record of a multistage evolution. Lithos 99, 207–228.

Baxter, E.F., Scherer, E.E., 2013. Garnet geochronology: timekeeper of tectonometamorphic processes. Elements 9, 433–438.

Baxter, E.F., Ague, J.J., Depaolo, D.J., 2002. Prograde temperature–time evolution in the Barrovian type–locality constrained by Sm/Nd garnet ages from Glen Clova, Scotland. Journal of the Geological Society 159, 71–82.

Baziotis, I., Mposkos, E., Perdikatsis, V., 2008. Geochemistry of amphibolitized eclogites and cross-cutting tonalitic-trondhjemitic dykes in the Metamorphic Kimi Complex in East Rhodope (NE Greece): implications for partial melting at the base of a thickened crust. International Journal of Earth Sciences 97 (3), 459–477.

Bhattacharya, A., Mohanty, I., Maji, A., Sen, S.K., Raith, M., 1992. Non-ideal mixing in the phlogopite-annite binary: constraints from experimental data on Mg—Fe partitioning and a reformulation of the biotite–garnet geothermometer. Contributions to Mineralogy and Petrology 111, 87–93.

Bonev, N., Stampfli, G., 2008. Petrology, geochemistry, and geodynamic implications of Jurassic island arc magmatism as revealed by mafic volcanic rocks in Mesozoic Low grade sequence of, Eastern Rhodope, Bulgaria. Lithos 100, 210–233.

Bonev, N., Stampfli, G., 2011. Alpine tectonic evolution of a Jurassic subduction–accretionary complex: deformation, kinematics and $^{40}Ar/^{39}Ar$ age constraints on the Mesozoic low-grade schists of the Circum–Rhodope Belt in the eastern Rhodope–Thrace region, Bulgaria-Greece. Journal of Geodynamics 52 (2), 143–167.

Bonev, N., Burg, J.P., Ivanov, Z., 2006. Mesozoic-Tertiary structural evolution of an extensional gneiss dome—the Kesebir-Kardamos dome, eastern Rhodope (Bulgaria-Greece). International Journal of Earth Sciences 95 (2), 318–340.
Bonev, N., Moritz, R., Marton, I., Chiaradia, M., Marchev, P., 2010. Geochemistry, tectonics, and crustal evolution of basement rocks in the Eastern Rhodope Massif, Bulgaria. International Geology Review 52, 269–297.
Bosse, V., Boulvais, P., Gautier, P., Tiepolo, M., Ruffet, G., Devidal, J.L., Cherneva, Z., Gerdjikov, I., Paquette, J.L., 2009. Fluid-induced disturbance of the monazite Th–Pb chronometer: in situ dating and element mapping in pegmatites from the Rhodope (Greece, Bulgaria). Chemical Geology 261, 286–302.
Bosse, V., Cherneva, Z., Gautier, P., Gerdjikov, I., 2010. Two partial melting events as recorded by the U-Th-Pb chronometer in monazite: LA-ICPMS in situ dating in metapelites from the Bulgarian Central Rhodopes. 19th Congress of the Carpathian-Balkan Geological Association, Thessaloniki, Greece 39, pp. 51–52.
Boyanov, I., Goranov, A., 2001. Late Alpine (Palaeogene) superimposed depressions in parts of South-east Bulgaria. Geologica Balcanica 31, 3–36.
Boyanov, I., Russeva, M., 1989. Lithostratigraphy and tectonic position of the Mesozoic rocks in the East Rhodopes: Geologica Rhodopica, v. 1. Postcollisional Tectonics and Magmatism in the Mediterranean Region and Asiapp. 22–33.
Burchfiel, B.C., 1980. Eastern European Alpine system and the Carpathian orocline as an example of collision tectonics. Tectonophysics 63, 31–61.
Burg, J.P., 2012. Rhodope: from Mesozoic convergence to Cenozoic extension. Review of petro-structural data in the geochronological frame. In: Skourtsos, Emmanuel, Lister, Gordon S. (Eds.), The geology of Greece. Journal of the Virtual Explorer, Electronic Edition1441-8142 42 (paper 1).
Burg, J.P., Ricou, L.-E., Ivanov, Z., Godfriaux, I., Dimov, D., Klain, L., 1996. Syn-metamorphic nappe complex in the Rhodope massif. Structure and kinematics. Terra Nova 8, 6–15.
Carlson, W.D., 2012. Rates and mechanisms of Y, REE, and Cr diffusion in garnet. American Mineralogist 97, 1598–1618.
Carrigan, C.W., Mukasa, S.B., Haydoutov, I., Kolcheva, K., 2003. Ion microprobe U–Pb zircon ages of pre-Alpine rocks in the Balkan, Sredna Gora and Rhodope terranes of Bulgaria: constraints on Neoproterozoic and variscan tectonic evolution. Journal of the Czech Geological Society 48, 32–33.
Carrigan, C.W., Mukasa, S.B., Haydoutov, I., Kolcheva, K., 2005. Age of Variscan magmatism from the Balkan sector of the orogen, central Bulgaria. Lithos 82, 125–147.
Chambers, J.A., Kohn, M.J., 2012. Titanium in muscovite, biotite, and hornblende: modeling, thermometry, and rutile activities of metapelites and amphibolites. American Mineralogist 97, 543–555.
Cherneva, Z., Georgieva, M., 2005. Metamorphozed Hercynian granitoids in the Alpine structures of the Central Rhodope, Bulgaria: geotectonic position and geochemistry. Lithos 82 (1-2), 149–168.
Chopin, C., 1984. Coesite and pure pyrope in high-grade blueschists of the Western Alps—a 1st record and some consequences. Contributions to Mineralogy and Petrology 86 (2), 107–118.
Collings, D., 2014. The tectono-metamorphic evolution of the Rhodope Massif, Bulgaria PhD Thesis, University of Leeds.
Didier, A., Bosse, V., Cherneva, Z., Gautier, P., Georgieva, M., Paquette, J.-L., Gerdjikov, I., 2014. Syn-deformation fluid assisted growth of monazite during renewed high grade metamorphism in metapelites of the Central Rhodope (Bulgaria, Greece). Chemical Geology 381, 206–222.
Dobrzhinetskaya, L.F., 2012. Microdiamonds—Frontier of ultrahigh-pressure metamorphism: a review. Gondwana Research 21 (1), 207–223.
Dragovic, B., Samanta, L.M., Baxter, E.F., Selverstone, J., 2012. Using garnet to constrain the duration and rate of water-releasing metamorphic reactions during subduction: an example from Sifnos, Greece. Chemical Geology 314, 9–22.
Duth, R., Hand, M., 2010. Retention of Sm–Nd isotopic ages in garnets subjected to high grade thermal reworking: implications for diffusion rates of major and rare earth elements and the Sm–Nd closure temperature in garnet. Contributions to Minerlaogy and Petrology 159, 93–112.
Ferry, J.T., Spear, F., 1978. Experimental calibration of the partitioning of Fe and Mg between biotite and garnet. Contributions to Mineralogy and Petrology 66, 113–117.
Gatewood, M.P., Dragovic, B., Stowell, H.H., Baxter, E.F., Hirsch, D.M., Bloom, R., 2015. Evaluating chemical equilibrium in metamorphic rocks using major element and Sm–Nd isotopic age zoning in garnet, Townshend Dam, Vermont, USA. Chemical Geology 401, 151–168.
Georgiev, S., Von Quadt, A., Heinrich, C., Peytcheva, I., Marchev, P., 2012. Time evolution of a rifted continental arc: integrated ID-TIMS and LA-ICPMS study of magmatic zircons from the Eastern Srednogorie, Bulgaria. Lithos 154, 53–67.
Georgieva, M., Cherneva, Z., Mogessie, A., Stancheva, E., 2007. Garnet–kyanite schists from the Chepelare area, Central Rhodopes Mts., Bulgaria: mineral chemistry, thermobarometry and indications for high-pressure melting. Proc. National Conf. Geosciences, pp. 97–98.
Guidotti, C.V., 1984. Micas in metamorphic rocks. Reviews in Mineralogy and Geochemistry 13, 357–467.
Hacker, B.R., Gerya, T.V., 2013. Paradigms, new and old, for ultrahigh-pressure tectonism. Tectonophysics 603, 79–88.
Harkovska, A., Yanev, Y., Marchev, P., 1989. General features of the Paleogene orogenic magmatism in Bulgaria. Geologica Balcanica 19, 37–72.
Harvey, J., Baxter, E.F., 2009. An improved method for TIMS high precision neodymium isotope analysis of very small aliquots (1–10 ng). Chemical Geology 258, 251–257.
Haydoutov, I., Kolcheva, K., Daieva, L.A., Savov, I.P., Carrigan, C., 2004. Island arc origin of the variegated formations from the East Rhodope, Bulgaria—implications for the evolution of the Rhodope Massif. Ofioliti 29 (2), 145–157.
Hsu, K.J., Nachev, I.K., Vuchev, V.T., 1977. Geologic Evolution of Bulgaria in light of plate tectonics. Tectonophysics 40 (3-4), 245–256.
Ivanov, Z., Moskovski, S., Dimov, D., Kolcheva, K., Klain, L., 1985. Geological structure of the Central Rhodopes. II. Structural sequences in the synmetamorphic evolution of the Central-Rhodope metamorphic group. Geologica Balcanica 15, 3–32.
Jahn-awe, S., Froitzheim, N., Nagel, T.J., Frei, D., Georgiev, N., Pleuger, J., 2010. Structural and geochronological evidence for Paleogene thrusting in the western Rhodopes, SW Bulgaria: elements for a new tectonic model of the Rhodope Metamorphic Province. Tectonics 29, TC3008.
Jahn-awe, S., Pleuger, J., Frei, D., Georgiev, N., Froitzheim, N., Nagel, T.J., 2012. Time constraints for low-angle shear zones in the Central Rhodopes (Bulgaria) and their significance for the exhumation of high-pressure rocks. International Journal of Earth Sciences 101, 1971–2004.
Janak, M., Froitzheim, N., Georgiev, N., Nagel, T.J., Sarov, S., 2011. P-T evolution of kyanite eclogite from the Pirin Mountains (SW Bulgaria): implications for the Rhodope UHP Metamorphic Complex. Journal of Metamorphic Geology 29 (3), 317–332.
Jolivet, L., Brun, J.-P., 2010. Cenozoic geodynamic evolution of the Aegean. International Journal of Earth Sciences 99, 109–138.
Jones, C.E., Tarney, J., Baker, J.H., Gerouki, F., 1992. Tertiary granitoids of Rhodope, northern Greece: magmatism related to extensional collapse of the Hellenic Orogen? Tectonophysics 210, 295–314.
Kirchenbaur, M., Pleuger, J., Jahn-Awe, S., Nagel, T., Froitzheim, N., Fonseca, R., Münker, C., 2012. Timing of high-pressure metamorphic events in the Bulgarian Rhodopes from Lu–Hf garnet geochronology. Contributions to Mineralogy and Petrology 163 (5), 897–921.
Konrad-Schmolke, M., O'Brien, P.J., Zack, T., 2011. Fluid migration above a subducted slub—constraints on amount, pathways and major element mobility from partially overprinted eclogite-facies rocks (Sesia Zone, Western Alps). Journal of Petrology 52, 457–486.
Korsakov, A.V., Zhukov, V.P., Vandenabeele, P., 2010. Raman-based geobarometry of ultrahigh-pressure metamorphic rocks: applications, problems, and perspectives. Analytical and Bioanalytical Chemistry 397 (7), 2739–2752.
Kostopoulos, D., Gerdjikov, I., Gautier, P., Reischmann, T., Cherneva, Z., 2003. First evidence of UHP metamorphism in the Central Rhodope Massif of southern Bulgaria. Geophysical Research Abstracts 5 (abstract 08327).
Krenn, K., Bauer, C., Proyer, A., Klotzli, U., Hoinkes, G., 2010. Tectonometamorphic evolution of the Rhodope orogen. Tectonics 29, TC4001.
Kretz, R., 1959. Chemical study of garnet, biotite, and hornblende from gneisses of southwestern Quebec, with emphasis on distribution of elements in coexisting minerals. The Journal of Geology 67 (4), 371–402.
Lee, J.K., Williams, I.S., Ellis, D.J., 1997. Pb, U and Th diffusion in natural zircon. Nature 390, 159–162.
Liati, A., 2005. Identification of repeated Alpine (ultra) high-pressure metamorphic events by U–Pb SHRIMP geochronology and REE geochemistry of zircon: the Rhodope zone of Northern Greece. Contributions to Mineralogy and Petrology 150 (6), 608–630.
Liati, A., Gebauer, D., Wisoczanski, D., 2002. U–Pb SHRIMP-dating of zircon domains from UHP garnet-rich mafic rocks and late pegmatoids in the Rhodope zone (N Greece): evidence for Early Cretaceous crystallization and Late Cretaceous metamorphism. Chemical Geology 184, 281–299.
Liati, A., Fanning, C.M., 2005. Eclogites and their country rock orthogneisses in East Rhodope representing upper permian gabbros and upper carboniferous granitoids: geochronological constraints. Abstract volume of the 7th International Eclogite Conference, Graz, Austria.
Liati, A., Gebauer, D., Fanning, C.M., 2011. Geochronology of the Alpine UHP Rhodope zone: a review of isotopic ages and constraints on the geodynamic evolution. In: Dobrzhinetskaya, L., Cuthbert, S. (Eds.), Ultrahigh Pressure Metamorphism 10. Elsevier, London, pp. 295–324.
Ludwig, K.R., 2003. User's manual for Isoplot 3.00: a geochronological toolkit for Microsoft Excel. Kenneth R. Ludwig.
Massonne, H.-J., Szpurka, Z., 1997. Thermodynamic properties of white micas on the basis of high-pressure experiments in the systems K_2O, MgO, Al_2O_3, SiO_2, H_2O and K_2O, FeO, Al_2O_3 SiO_2, H_2O. Lithos 41, 229–250.
Mezger, K., Essene, E.J., Halliday, A., 1992. Closure temperatures of the Sm—Nd system in metamorphic garnets. Earth and Planetary Science Letters 113, 397–409.
Mposkos, E.D., Kostopoulos, D.K., 2001. Diamond, former coesite and supersilicic garnet in metasedimentary rocks from the Greek Rhodope: a new ultrahigh-pressure metamorphic province established. Earth and Planetary Science Letters 192 (4), 497–506.
Nagel, T.J., Schmidt, S., Janák, M., Froitzheim, N., Jahn-awe, S., Georgiev, N., 2011. The exposed base of a collapsing wedge: the Nestos shear zone (Rhodope Metamorphic Province, Greece). Tectonics 30, TC4009.
Naydenov, K., Von Quadt, A., Peytcheva, I., Sarov, S., Dimov, D., 2009. U–Pb zircon dating of metamorphic rocks in the region of Kostenets-Kozarsko villages: constraints on the tectonic evolution of the Maritsa strike-slip shear zone. The Review of the Bulgarian Geological Society 70, 5–21.
Ovtcharova, M., Von Quadt, A., Cherneva, Z., Sarov, S., Heinrich, C., Peytcheva, I., 2004. U–Pb dating of zircon and monazite from granitoids and migmatites in the core and eastern periphery of the Central Rhodopean Dome, Bulgaria. Geochimica et Cosmochimica Acta 68 (11), A664.
Papanikolaou, D., 1997. The tectonostratigraphic terranes of the Hellenides. Annales Géologiques des Pays Helléniques 495–514.
Perraki, M., Proyer, A., Mposkos, E., Kaindl, R., Hoinkes, G., 2006. Raman microspectroscopy on diamond, graphite and other carbon polymorphs from the ultrahigh-pressure metamorphic Kimi Complex of the Rhodope Metamorphic Province, NE Greece. Earth and Planetary Science Letters 241 (4), 672–685.
Peytcheva, I., von Quadt, A., Georgiev, N., Ivanov, Z., Heinrich, C., Frank, M., 2008. Combining trace element compositions, U–Pb geochronology and Hf isotopes in zirocns to

unravel complex calcalkaline magma chambers in the Upper Cretaceous Srednogorie zone (Bulgaria). Lithos 104, 405–427.
Pollington, A.D., Baxter, E.F., 2011. High precision microsampling and preparation of zoned garnet porphyroblasts for Sm–Nd geochronology. Chemical Geology 281, 270–282.
Reischmann, T., Kostopoulos, D., 2002. Timing of UHPM in metasediments from the Rhodope Massif, N Greece. Proceedings Goldschmidt Conf., Davos, Switzerland, abstract A634.
Ricou, L.E., Burg, J.P., Godfriaux, I., Ivanov, Z., 1998. Rhodope and Vardar: the metamorphic and the olistostromic paired belts related to the Cretaceous subduction under Europe. Geodinamica Acta 11 (6), 285–309.
Rubatto, D., 2002. Zircon trace element geochemistry: partitioning with garnet and the link between U–Pb ages and metamorphism. Chemical Geology 184, 123–138.
Sarov, S., 2004. Geological Map of Republic of Bulgaria 1: 50 000 , sheet K 35- 74 B Bulgarian National Geological Survey, (Project 425/20/07. 2004).
Savov, I.P., Bizimis, M., Halama, R., Shirey, S., Hauri, E., Haydoutov, I., 2007. Li–Sr–Lu–Hf isotope and trace element systematics of eclogites from Bulgaria. Geochimica et Cosmochimica Acta 71 (15), A879.
Schmidt, S., Nagel, T.J., Froitzheim, N., 2010. A new occurrence of microdiamond-bearing metamorphic rocks, SW Rhodopes, Greece. European Journal of Mineralogy 22 (2), 189–198.
Smit, M.A., Scherer, E.E., Mezger, K., 2013. Lu–Hf and Sm–Nd garnet geochronology: chronometric closure and implications for dating petrological processes. Earth and Planetary Science Letters 381, 222–233.
Sobolev, N.V., Shatsky, V.S., 1990. Diamond inclusions in garnets from metamorphic rocks—a new environment for diamond formation. Nature 343, 742–746.
Stampfli, G., Borel, G., 2002. A plate tectonic model for the Paleozoic and Mesozoic constrained by dynamic plate boundaries and restored synthetic oceanic isochrons. Earth and Planetary Science Letters 196, 17–33.
Tomkins, H.S., Powell, R., Ellis, D.J., 2007. The pressure dependance of the Zirconium-in-rutile thermometer. Journal of Metamorphic Geology 25, 701–713.
Turpaud, P., Reischmann, T., 2010. Characterisation of igneous terranes by zircon dating: implications for UHP occurrences and suture identification in the Central Rhodope, northern Greece. International Journal of Earth Sciences 99 (3), 567–591.
Von Quadt, A., Moritz, R., Peytcheva, I., Heinrich, C.A., 2005. Geochronology and geodynamics of Late Cretaceous magmatism and Cu–Au mineralization in the Panagyurishte region of the Apuseni–Banat–Timok–Srednogorie belt, Bulgaria. Ore Geology Reviews 27, 95–126.
Von Quadt, A., Sarov, S., Peytcheva, I., Voynova, I., Petrov, N., Nedkova, K., Naydenov, K., 2006. Metamorphic rocks from northern parts of Central Rhodopes—conventional and in situ U–Pb zircon dating, isotope tracing and correlations. National Conference "Geosciences 2006", Bulgarian Geological Society, Sofia, pp. 225–228.
Warren, C., 2013. Exhumation of (ultra-) high pressure terranes: concepts and Mechanims. Solid Earth 4, 75–92.
Wawrzenitz, N., Mposkos, E., 1997. First evidence for Lower Cretaceous HP/HT-metamorphism in the eastern Rhodope, North Aegean region, North-east Greece. European Journal of Mineralogy-Ohne Beihefte 9, 659–664.
Wendt, I., Carl, C., 1991. The statistical distribution of the mean squared weighted deviation. Chemical Geology (Isotope Geoscience Section) 86, 275–285.
Zack, T., Moraes, R., Kronz, A., 2004. Temperature dependence of Zr in rutile: empirical calibration of a rutile thermometer. Contributions to Mineralogy and Petrology 148 (4), 471–488.
Zidarov, N.G., Nenova, P.I., Dimov, V.I., 1995. Coesite in kyanite eclogite of Ograzden MTS, SW Bulgaria. Comptes Rendus de l'Académie Bulgare des Sciences 48, 59–62.